

This document is confidential and is proprietary to the American Chemical Society and its authors. Do not copy or disclose without written permission. If you have received this item in error, notify the sender and delete all copies.

**An Interatomic Potential for Hydrocarbons Based on the Modified Embedded-Atom Method with Bond Order (MEAM-BO)**

Journal:	<i>The Journal of Physical Chemistry</i>
Manuscript ID	jp-2016-11343n.R1
Manuscript Type:	Article
Date Submitted by the Author:	n/a
Complete List of Authors:	Mun, Sungkwang; Mississippi State University, Center for Advanced Vehicular Systems Bowman, Andrew; Mississippi State University, Center for Advanced Vehicular Systems Nouranian, Sasan; The Univeristy of Mississippi, Chemical Engineering Gwaltney, Steven; Mississippi State University, Chemistry Baskes, Michael; MSU, Aerospace Engineering Horstemeyer, Mark; Mississippi State University, Mechanical Engineering

SCHOLARONE™  
Manuscripts

1 **Title:** An Interatomic Potential for Hydrocarbons Based on the Modified Embedded-Atom Method with Bond  
2 Order (MEAM-BO)  
3  
4  
5  
6

7 **Authors:** Sungkwang Mun<sup>a</sup>, Andrew L. Bowman<sup>a</sup>, Sasan Nouranian<sup>b</sup>, Steven R. Gwaltney<sup>c</sup>, Michael I.  
8 Baskes<sup>\*,d,e,f,g</sup>, and Mark F. Horstemeyer<sup>a,h</sup>  
9

10  
11 <sup>a</sup>: Center for Advanced Vehicular Systems (CAVS), Mississippi State University,  
12 Mississippi State, MS 39762, USA  
13  
14

15 <sup>b</sup>: Department of Chemical Engineering, The University of Mississippi, MS 38677, USA  
16  
17

18 <sup>c</sup>: Department of Chemistry, Mississippi State University, Mississippi State,  
19 MS 39762, USA  
20  
21

22 <sup>d</sup>: Department of Aerospace Engineering, Mississippi State University,  
23 Mississippi State, MS 39762, USA.  
24  
25

26 <sup>e</sup>: Los Alamos National Laboratory, NM 87545, USA  
27  
28

29 <sup>f</sup>: Department of Mechanical and Aerospace Engineering, University of California, CA 92093, USA  
30  
31

32 <sup>g</sup>: Department of Materials Science and Engineering, University of North Texas, TX 76203, USA  
33  
34

35 <sup>h</sup>: Department of Mechanical Engineering, Mississippi State University,  
36 Mississippi State, MS 39762, USA  
37  
38

39 <sup>\*</sup>: Corresponding author (Phone: 1-760-707-9483)  
40  
41

42 Email addresses: [sungkwan@cavs.msstate.edu](mailto:sungkwan@cavs.msstate.edu), [andrewb@cavs.msstate.edu](mailto:andrewb@cavs.msstate.edu), [sasan@olemiss.edu](mailto:sasan@olemiss.edu),  
43 [sgwaltney@chemistry.msstate.edu](mailto:sgwaltney@chemistry.msstate.edu), [baskes@bagley.msstate.edu](mailto:baskes@bagley.msstate.edu), [mforst@me.msstate.edu](mailto:mforst@me.msstate.edu)  
44  
45  
46  
47  
48  
49  
50  
51  
52  
53  
54  
55  
56  
57  
58  
59  
60

## Abstract

1  
2  
3 In this paper, we develop a new Modified Embedded Atom Method (MEAM) potential that includes the  
4 bond order (MEAM-BO) to describe the energetics of unsaturated hydrocarbons (double and triple carbon  
5 bonds) and also develop improved parameters for saturated hydrocarbons from those of our previous work.  
6  
7 Such quantities like bond lengths, bond angles, and atomization energies at 0 K, dimer molecule interactions,  
8 rotational barriers, and the pressure-volume-temperature relationships of dense systems of small molecules give  
9 a comparable or more accurate property relative to experimental and first-principles data than the classical  
10 reactive force fields REBO and ReaxFF. Our extension of the MEAM potential for unsaturated hydrocarbons  
11 (MEAM-BO) is a step towards developing more reliable and accurate polymer simulations with their associated  
12 structure-property relationships, such as reactive multicomponent (organic/metal) systems, polymer-metal  
13 interfaces, and nanocomposites. When the constants for the BO are zero, MEAM-BO reduces to the original  
14 MEAM potential. As such, this MEAM-BO potential describing the interaction of organic materials with  
15 metals within the same MEAM formalism is a significant advancement for computational materials science.  
16  
17  
18  
19  
20  
21  
22  
23  
24  
25  
26  
27  
28  
29  
30  
31  
32  
33  
34  
35

## 1. Introduction

36  
37  
38 Since interatomic potentials are at the heart of atomistic and molecular simulations, the advancement of  
39 materials diversity and computational interest has growingly translated into more sophisticated potentials that  
40 can provide accurate descriptions between different constituent elements' atomic interactions. These  
41 interactions provide the basis for the calculation of material properties of interest. The situation has escalated  
42 even more with a growing scientific and technological interest in alloys and composite/multi-layer materials  
43 that are made of two or more constituent elements. The interface between dissimilar materials introduces a  
44 whole new set of fundamental scientific problems that need to be solved. Currently, interfacial and interphase  
45 engineering are at the forefront of scientific research in different disciplines within automotive, aerospace,  
46 military, and biomedical industries.<sup>1-6</sup> Researchers need to tackle many hitherto unresolved scientific issues  
47  
48  
49  
50  
51  
52  
53  
54  
55  
56  
57  
58  
59  
60

1 related to molecular mechanisms involved in the observed macroscopic material properties; as a consequence,  
2 establishing fundamental composition-microstructure-property relationships is a critical need. However, a  
3 scientific gap exists today, wherein interatomic potentials that can reliably and accurately reproduce and predict  
4 the myriad of properties associated with complex single- and multi-component, multi-element material systems  
5 are non-existent or are available with limited applicability. The current work's significance is the development  
6 of an extensive interatomic potential based on a promising Modified Embedded Atom Method (MEAM)  
7 formalism.<sup>7</sup> The MEAM potential is a modification to the original Embedded-Atom Method (EAM), developed  
8 by Daw and Baskes<sup>8</sup> in 1984, that includes a formalism for covalent materials (directional bonding), such as  
9 silicon and silicon-germanium alloys. Both EAM and MEAM potentials are widely used by computational  
10 materials scientists and engineers conducting atomistic simulations related to point defects, melting, alloying,  
11 grain boundary structure and energy, dislocations, twins, segregation, fracture, surface structure, epitaxial  
12 growth, bulk and interface problems (surface phonons), and inter-diffusion in metallic alloys. The unique  
13 feature of MEAM is its ability to reproduce the physical properties of a large number of crystal structures in  
14 unary, binary, ternary, and higher order metal systems with the same formalism. The recent development<sup>9</sup> by  
15 the authors shows MEAM successfully extended to saturated hydrocarbons without any modification to the  
16 original formalism, which gives a possibility to study multi-element systems based the vast parameter database  
17 of metals.

18  
19  
20  
21  
22  
23  
24  
25  
26  
27  
28  
29  
30  
31  
32  
33  
34  
35  
36  
37  
38  
39  
40 As a continuation of the previous work of Nouranian *et al.*,<sup>9</sup> we developed here a new formalism for  
41 unsaturated bond energies and added to the existing MEAM formalism. Furthermore, we improved the results  
42 of previous works that are not related to bond order through the following: 1) a critical issue in the carbon (C)  
43 parameters of the previous work has been fixed so that the diamond cubic structure (reference structure for C) is  
44 energetically more stable than the face-centered cubic (FCC) and body-centered cubic (BCC) crystal structures;  
45 2) partial contributions of third nearest neighbor (3NN) interactions<sup>10</sup> are considered in the C reference structure,  
46 which allows for more accurate diamond properties than those predicted by the previous parameters; 3) the  
47 reference structure for CH has been changed from the CH dimer to methane, which improves the agreement  
48  
49  
50  
51  
52  
53  
54  
55  
56  
57  
58  
59  
60

with the hydrocarbons experimental data.

This paper is organized in the following manner. In Section 2, the MEAM formalism including its bond terms and the potential development are presented. The results are given in Section 3, followed by the conclusion in Section 4.

## 2. Methodology

### 2.1 MEAM formalism

In this work, we used the Modified Embedded-Atom Method (MEAM) potential, which is a reactive semi-empirical many body potential based on density functional theory<sup>7,8,11,12</sup>. Since it was first introduced in 1992, the MEAM potential has successfully been used to calculate the physical properties of a large number of FCC, BCC, HCP, and diamond cubic crystal structures in unary, binary, ternary, and higher-order metallic systems. Also, a recent study<sup>9</sup> showed that the same MEAM formalism gives a reasonable prediction of the energies for a series of methane, ethane, propane, and butane systems without any modification to the original form of the equations.

Although the formalism is explained in more detail in Nouranian *et al.*<sup>9</sup> and Baskes,<sup>11</sup> a brief explanation of the MEAM formalism follows. The mathematical notations used in this paper are  $f(\cdot)$  is a function,  $i$  (parentheses in a superscript) is an index, and  $\cdot$  (centered dot) is multiplication. The total energy of a system is approximated as the sum of the energy over all atoms,  $i$ .

$$E_{\text{MEAM}} = \sum_i E_i \quad (1)$$

The energy of atom  $i$  consists of 1) an embedding energy and 2) a pair interaction energy with 3) a screening function given by the following,

$$E_i = F_\tau(\bar{\rho}_i) + \frac{1}{2} \sum_{j \neq i} S_{ij} \cdot \phi_{\tau_i \tau_j}(R_{ij}) \quad (2)$$

- 1) The embedding function, representing the energy cost to insert an atom  $i$  of element type  $\tau$  (i.e. C or H) at a site with background electron density  $\bar{\rho}_i$ , is expressed as follows:

$$F_{\tau}(\bar{\rho}_i) = A_{\tau} \cdot E_{\tau}^0 \cdot \frac{\bar{\rho}_i}{\bar{\rho}_{\tau}^0} \cdot \ln\left(\frac{\bar{\rho}_i}{\bar{\rho}_{\tau}^0}\right) \quad (3)$$

where  $A_{\tau}$  is a parameter dependent on the element type  $\tau$ ,  $E_{\tau}^0$  is the cohesive energy of the reference structure of the element type  $\tau$ ,  $\bar{\rho}_{\tau}^0$  is the equilibrium background electron density for the reference structure, and  $\bar{\rho}_i$  is the total background electron density at the site of atom  $i$ . We note here that superscripts do not denote contravariant Einsteinian notation but only represent a descriptor throughout the text. The term  $\bar{\rho}_i$  is given by the combination of the partial electron densities of a spherically symmetric term  $\rho_i^{(0)}$  and three angular terms  $\rho_i^{(1-3)}$  in Nouranian *et al.*<sup>9</sup>

$$\bar{\rho}_i = \rho_i^{(0)} \cdot G(\Gamma_i). \quad (4)$$

Here,  $G$  is an auxiliary function to handle a negative value that may arise at certain geometries of the system. In this work we used the sign-preserving square root form given below,

$$G(\Gamma) = \begin{cases} \sqrt{1+\Gamma} & 1+\Gamma \geq 0 \\ -\sqrt{|1+\Gamma|} & 1+\Gamma < 0 \end{cases} \quad (5)$$

$\Gamma_i$  is the sum of all angular terms of partial electron density given by

$$\Gamma_i = \sum_{h=1}^3 \bar{t}_i^{(h)} \cdot \left[ \frac{\rho_i^{(h)}}{\rho_i^{(0)}} \right]^2, \quad (6)$$

where  $\bar{t}_i^{(h)}$  ( $h = \{1,2,3\}$ ) is a scaling factor. The equation for  $\bar{t}_i^{(h)}$  is found in Nouranian *et al.*<sup>9</sup>. Finally, the atomic electron density in each partial charge density  $\rho_i^{(h)}$  is given by

$$\rho_{\tau}^{a(h)}(R_{ij}) = \rho_{\tau}^0 \cdot \exp\left(-\beta_{\tau}^{(h)} \cdot \left[\frac{R_{ij}}{R_{\tau}^0} - 1\right]\right), \quad (7)$$

where  $\rho_{\tau}^0$  is an element-dependent electron density scaling factor,  $\beta_{\tau}^{(h)}$  ( $h = \{0,1,2,3\}$ ) are four parameters that describes the decay of the electron density with respect to the distance  $R_{ij}$ , and  $R_{\tau}^0$  is the equilibrium nearest neighbor distance in the reference phase.

2) As for the pair interaction, MEAM does not have a specific functional expression, but the energy per atom for the reference structure is given as a function of first nearest neighbor distances (1NN). In this work, H<sub>2</sub> for the H-H interaction, diamond cubic for the C-C interaction, and CH<sub>4</sub> for the C-H interaction are utilized as reference structures. The energy of the reference structure,  $E^u$  is given by the universal equation of state (UEOS) of Rose *et al.*<sup>13</sup> with respect to the nearest neighbor distance  $R_{ij}$

$$E^u(R_{ij}) = -E_{\text{REF}}^0 \cdot \left[ 1 + a^*(R_{ij}) + \delta_{\text{REF}} \cdot \frac{R_{\text{REF}}^0}{R_{ij}} \cdot a^*(R_{ij})^3 \right] \cdot e^{-a^*(R_{ij})}, \quad (8)$$

where  $\delta_{\text{REF}} = \begin{cases} \delta_{\text{REF}}^a, & \text{if } a^* \geq 0 \\ \delta_{\text{REF}}^r, & \text{if } a^* < 0 \end{cases}$ , and  $a^*(R_{ij}) = \alpha_{\text{REF}}^0 \cdot \left[ \frac{R_{ij}}{R_{\text{REF}}^0} - 1 \right]$ . Here, the parameters  $E_{\text{REF}}^0$ ,  $R_{\text{REF}}^0$ ,  $\alpha_{\text{REF}}^0$ ,

$\delta_{\text{REF}}^a$ , and  $\delta_{\text{REF}}^r$  are obtained from the reference structure (REF=C, H, and CH).

Another consideration for the pair interaction is that each pair interaction energy is calculated either by only considering the 1NN interactions<sup>11</sup> or by considering the partial contribution of the second or third nearest neighbor (2NN or 3NN)<sup>14</sup> interactions as well as the 1NN interaction, depending on the reference structure. The pair interaction for like-atoms of element type  $\tau$  by interacting by 1NN only (H) is given by

$$\phi_{\tau\tau}(R_{ij}) = \frac{2}{Z_{1,\tau}^0} \cdot [E^u(R_{ij}) - F_{\tau}(\bar{\rho}_{\tau}^{\text{ref}})], \quad (9)$$

where  $Z_{1,\tau}^0$  is the 1NN coordination number of the reference structure (e.g. one for H<sub>2</sub>),  $F_{\tau}(\cdot)$  is the embedding function in Eq. (3), and  $\bar{\rho}_{\tau}^{\text{ref}}$  is the background electron density in the reference structure obtained from Eq. (4). Because the reference structure for H in this work is H<sub>2</sub>, H only has 1NN interactions, but since we choose the diamond cubic structure for C, more distant interactions may enter. We have found that first 3NN then 2NN become unscreened as the screening (discussed below) is weakened. In order for a better description of C behavior, especially the elastic constants, 3NN interactions are considered in the sum of pair potentials  $\psi$ . Following Eq. (16) of Lee *et al.*<sup>14</sup>

$$\psi(R_{ij}) = \phi_{\tau\tau}(R_{ij}) + \frac{Z_{3\text{NN}}^0}{Z_{1\text{NN}}^0} \cdot S_{ij}^{3\text{NN}} \cdot \phi_{\tau\tau}(a \cdot R_{ij}) \quad (10)$$

Here,  $Z_{1\text{NN}}^0$  and  $Z_{3\text{NN}}^0$  are the number of 1NN and 3NN atoms, respectively (4 and 12 for diamond cubic),  $a$  is the ratio between 3NN and 1NN distances ( $\sqrt{11/3}$  for diamond cubic), and  $S_{ij}^{3\text{NN}}$  is the screening function for 3NN (discussed below). The rest of the derivation follows Lee *et al.*<sup>14</sup>.

The pair interaction for unlike atoms of element type  $\tau$  and  $\nu$  is obtained from the reference structure of unlike atoms. The reference structure for unlike atoms for this work is CH<sub>4</sub> (methane). The screening is chosen so that the H-H interactions are completely screened. In that case, for  $\tau=\text{C}$  and  $\nu=\text{H}$ , the pair interaction equation is given by

$$\phi_{\tau\nu}(R_{ij}) = \frac{1}{Z_{\tau\nu}^0} \cdot \left[ 5E^u(R_{ij}) - F_{\tau} \left( \rho_{\nu}^{a(0)}(R_{ij}) \cdot G \left( \Gamma_{\nu}^d(R_{ij}) \right) \right) - 4F_{\nu} \left( \rho_{\tau}^{a(0)}(R_{ij}) \cdot G \left( \Gamma_{\tau}^d(R_{ij}) \right) \right) \right], \quad (11)$$

where  $Z_{\tau\nu}^0=4$  is the coordination number of the carbon in CH<sub>4</sub>, and

$$\Gamma_{\tau}^d(R_{ij}) = \sum_{h=1}^3 t_{\tau}^{(h)} \cdot s_{\tau}^{(h)} \cdot \left[ \frac{\rho_{\tau}^{a(h)}(R_{ij})}{\rho_{\tau}^{a(0)}(R_{ij})} \right]^2, \quad (12)$$

where  $t_{\tau}^{(h)}$  are three adjustable parameters, and  $s_{\tau}^{(h)}$  are shape factors of the perfect lattice of the structure specified in Baskes<sup>11</sup>. In this work,  $s_{\tau}^{(1)}=0$ ,  $s_{\tau}^{(2)}=0$ , and  $s_{\tau}^{(3)}=32/9$  are used for C.  $\Gamma_{\nu}^d$  is also similarly obtained, and  $s_{\nu}^{(1)}=1$ ,  $s_{\nu}^{(2)}=2/3$ , and  $s_{\nu}^{(3)}=1$  are used for H.

- 3) The total screening function is the product of a radial cutoff function and three body terms involving all the other atoms in the system:

$$S_{ij} = \bar{S}_{ij} \cdot f_c \left( \frac{1-R_{ij}/R_c}{1-\Delta r_c} \right) \quad (13)$$

where  $\bar{S}_{ij}$  is the product of all screening factors  $S_{ikj}$ ,  $f_c$  is a smooth cutoff function,  $R_c$  is the cutoff distance, and  $\Delta r_c$  is a parameter that controls the distance over which the radial cutoff is smoothed from 1 to 0 near  $R_{ij}=R_c$ . In this work, we used  $R_c=5\text{\AA}$  throughout all tests except the graphite elastic constants calculations where we used  $R_c=6\text{\AA}$ , and  $\Delta r_c=0.9$ .  $S_{ij}=1$  means the atoms  $i$  and  $j$  are unscreened and within the cutoff distance, while  $S_{ij}=0$  means the atoms  $i$  and  $j$  are completely screened or outside the cutoff.

Finally,  $S_{ikj}$  is calculated as follows,

$$S_{ikj} = f_c \left( \frac{C_{ikj} - C_{\min}(\tau_i, \tau_k, \tau_j)}{C_{\max}(\tau_i, \tau_k, \tau_j) - C_{\min}(\tau_i, \tau_k, \tau_j)} \right) \quad (14)$$

where  $f_c$  is a smooth cutoff function, and  $C_{\min}(\tau_i, \tau_k, \tau_j)$  and  $C_{\max}(\tau_i, \tau_k, \tau_j)$  determine the extent of screening of atoms of element type  $\tau$  at sites  $i$  and  $j$  by an atom at site  $k$ . The equation for  $f_c$  and  $C_{ikj}$  used here are found in Nouranian *et al.*<sup>9</sup>

One significant challenge to the MEAM potential in Nouranian *et al.*<sup>9</sup> is the lack of capability to distinguish bond order in different type of molecules, such as acetylene (bond order 3), ethylene (2), benzene (3/2), and graphene (4/3). One solution to this challenge is to assign a fraction of both double and triple bond characters to each bond  $I$  between atoms  $i_1$  and  $i_2$ . We denote these fractions as  $f_{I2}$  for the double bond character and  $f_{I3}$  for the triple bond character. If the bond is saturated, i.e., a single bond, these fractions are both zero. A perfect double bond would have  $f_{I2} = 1$  and  $f_{I3} = 0$ , and a perfect triple bond would have  $f_{I2} = 0$  and  $f_{I3} = 1$ . Using this concept, we modify the standard MEAM energy as follows:

$$E_{\text{MEAM-BO}} = E_{\text{MEAM}} + \sum_I f_{I3} \cdot E_3(R_I) + \sum_I f_{I2} \cdot E_2(R_I, BO_I) \quad (15)$$

$E_{\text{MEAM}}$  is the energy from the MEAM formalism in Nouranian *et al.*<sup>9</sup> and Baskes<sup>11</sup> as given in Eq. (1).  $E_{\text{bond}}$  is the increment of energy due to the bond unsaturation, i.e., going from a single bond to a double bond ( $E_{\text{bond}=2}$ ) or to a triple bond ( $E_{\text{bond}=3}$ ). For both the double and triple bonds,  $E_{\text{bond}}$  depends on  $R_I$ , the bond length, i.e.  $R_I = R_{i_1 i_2}$ . In addition, for the double bond,  $E_2$  also depends on the bond order,  $BO_I$ , which must lie between 1 and 2. The energy fraction for the triple bond is given by

$$f_{I3} = S_{i_1 i_2} \cdot D_3^{(0)} \left( [Z_{i_1}^{(0)} - Z_3]^2 \right) \cdot D_3^{(0)} \left( [Z_{i_2}^{(0)} - Z_3]^2 \right) \cdot D_3^{(3)} \left( [Z_I^{(3)}]^2 \right), \quad (16)$$

where  $S_{i_1 i_2}$  is the angular screening function for the two atoms in the bond.  $Z_i^{(0)}$  is an atom counting factor that we define below. For a triple bond, each atom ( $i_1$  and  $i_2$ ) must have two neighboring atoms ( $Z_3 = 2$ ) so the energy fraction is reduced by a function,  $D_{\text{bond}}^{(h)}$ , which has a maximum of unity when the argument is zero and approaches zero rapidly when the argument moves away from zero. The choice for  $D_{\text{bond}}^{(h)}$  in this work is a

modified Gaussian function given below. In addition, as the molecule varies away from linearity, the bond type changes from a triple to a double bond. The final term captures this effect for the triple bond, where the atom counting factor  $Z_I^{(3)}$ , defined below, is centered at the bond  $I$ , which is considered an entity and is located halfway between the two atoms that compose the bond. Note that if the two atoms of the bond are of the same type, this definition of bond center makes sense, but if the atoms are of different types, a more general definition of bond center may be required. In this work, however, we consider only bonds between two C atoms, and hence do not need to consider this issue.

On the other hand, each atom of a double bond requires three neighboring atoms ( $Z_2 = 3$ ) that are planar, and the planes for the two atoms that constitute the bond must be parallel. In this case, the energy fraction is given by the sum of two terms,

$$f_{I2} = S_{i_1 i_2} \cdot D_2^{(0)} \left( [Z_{i_1}^{(0)} - Z_2]^2 \right) \cdot D_2^{(0)} \left( [Z_{i_2}^{(0)} - Z_2]^2 \right) \cdot D_2^{(1)} \left( [Z_{i_1}^{(1)}]^2 \right) \cdot D_2^{(1)} \left( [Z_{i_2}^{(1)}]^2 \right) \cdot D_2^{(3)} \left( [Z_I^{(3)}]^2 \right) + f_{I3} \cdot \left( 1 - D_3^{(3)} \left( [Z_I^{(3)}]^2 \right) \right), \quad (17)$$

where the first term satisfies the geometric constraints, and the second term is the transfer of bond type from a triple to a double bond discussed above. We have defined an additional atom counting factor  $Z_i^{(1)}$  at each atom. The geometric conditions are satisfied if  $Z^{(0)} \sim 3$ ,  $Z^{(1)} \sim 0$ , and  $Z^{(3)} \sim 0$ .

The counting factors are given by equations similar to those used for MEAM partial electron densities in Nouranian *et al.*,<sup>9</sup> where, as usual, the density at an atom does not include contributions from that atom, and similarly the background electron density at the bond center does not include contributions from the atoms that form the bond.

$$Z_i^{(0)} = \sum_{j \neq i} S_{ij}, \quad (18)$$

$$[Z_i^{(1)}]^2 = \sum_{\alpha} \left[ \sum_{j \neq i} \frac{R_{ij}^{\alpha}}{R_{ij}} \cdot S_{ij} \right]^2, \quad (19)$$

and

$$[Z_I^{(3)}(R_{Ij})]^2 = \sum_{\alpha, \beta, \gamma} \left[ \sum_{j \neq i_1, i_2} \frac{R_{Ij}^{\alpha} \cdot R_{Ij}^{\beta} \cdot R_{Ij}^{\gamma}}{R_{Ij}^3} \cdot S_{Ij} \right]^2 - \frac{3}{5} \sum_{\alpha} \left[ \sum_{j \neq i_1, i_2} \frac{R_{Ij}^{\alpha}}{R_{Ij}} \cdot S_{Ij} \right]^2. \quad (20)$$

Here,  $S_{Ij}$  is the total screening function between the center of bond  $I$  and atom  $j$  similar to Eq. (13), and  $R_{Ij}^{\alpha/\beta/\gamma}$  is the  $\alpha$ ,  $\beta$ , and  $\gamma$  components of the distance vector between the center of bond  $I$  and atom  $j$ . In the calculation of these atom counting factors, the radial cutoff used in the calculation of the screening  $S_{Ij}$  (see Eq. (13)) is decreased to a distance somewhat less than the van der Waals diameter of the atom type in the bond. In this work, this distance ( $\hat{r}_{vdW}$ ) is taken as 3.30 Å for C which is slightly less than the distance between two sheets (A-B stacking distance, 3.35 Å) in the graphite structure.

For the double and triple bonds, the attenuation function at the bond center is described as the following,

$$D_{\text{bond}}^{(h)}(Z) = \exp\left(-Z^{p_{\text{bond}}^{(h)}} \cdot \beta_{\text{bond}}^{(h)}\right), \quad (21)$$

where  $\beta_{\text{bond}}^{(h)}$  and  $p_{\text{bond}}^{(h)}$  represent six adjustable parameters ( $h = \{0,1,3\}$ ). Finally, the bond energy increment,  $E_{\text{bond}}$ , in Eq. (15) is calculated based on the energy versus the bond distance (triple bond) or the energy versus the bond distance and the bond order (double bond). Here, we start with the triple bond case first due to its simpler expression. The reference state for triple bond is acetylene ( $\text{C}_2\text{H}_2$ ). An expansion around the equilibrium bond length gives the following expression,

$$E_3(R_I) = e_0 \cdot \left\{ 1 + \sum_{k=1}^2 e_k \cdot \left[ \frac{R_I}{R_3} - 1 \right]^k \right\} \cdot \exp\left(-\beta_3^{(2)} \cdot \left[ \frac{R_I}{R_3} - 1 \right]\right) + [1 - S_{i_1 i_2}] \cdot E_{\text{vdW}}(R_I) \quad (22)$$

where  $e_k$  ( $k = \{0,1,2\}$ ) and  $\beta_3^{(2)}$  are parameters used to fit the bond length dependence for the reference state (in this case  $\text{C}_2\text{H}_2$ ), and  $R_3$  is the experimental triple bond length, e.g. 1.203 Å for  $\text{C}_2\text{H}_2$ . The second term of the equation includes the van der Waals energy increment, which is explained later in this section. The bond

energy increment for the double bond has a little more complex form to deal with the different bond order.

Three reference states for double bonds, ethylene ( $C_2H_4$ ), benzene, and graphene, are used. Similarly for the double bond, an expansion around the equilibrium bond length gives the following expression,

$$E_2(R_I, BO_I) = e_0(BO_I) \cdot \left\{ 1 + \sum_{k=1}^2 e_k(BO_I) \cdot \left[ \frac{R_I}{R_2(BO_I)} - 1 \right]^k \right\} \cdot \exp \left( -\beta_2^{(2)} \cdot \left[ \frac{R_I}{R_2(BO_I)} - 1 \right] \right) + [1 - S_{i_1 i_2}] \cdot E_{vdW}(R_I), \quad (23)$$

where  $e_k$  and  $\beta_2^{(2)}$  are parameters used to fit the bond length dependence for each of the three reference states, and the experimental double bond length,  $R_2(BO_I)$ , as a function of bond order is given by:

$$R_2(BO_I) = \sum_{l=0}^2 r_l \cdot [BO_I - 2]^l \quad (24)$$

where the  $r_l$  are parameters. The three reference states for the double bond are given by an expansion around the perfect double bond:

$$e_k(BO_I) = \sum_{l=0}^2 g_{kl} \cdot [BO_I - 2]^l \quad (25)$$

where  $g_{kl}$  are parameters. The bond order,  $BO_I$ , is calculated by counting neighbors of each atom of the bond.

$$BO_I = \frac{2 + n_I}{n_I} \quad (26)$$

where  $n_I$  is the sum of the partial contribution over  $j$  includes all neighbors of atoms  $i_1$  and  $i_2$ ,

$$n_I = \max \left( 2, \sum_{j \neq i_1} S_{i_1 j} \cdot D_2^{(0)} \left( [Z_j^{(0)} - Z_2]^2 \right) \cdot D_2^{(1)} \left( [Z_j^{(1)}]^2 \right) + \sum_{j \neq i_2} S_{i_2 j} \cdot D_2^{(0)} \left( [Z_j^{(0)} - Z_2]^2 \right) \cdot D_2^{(1)} \left( [Z_j^{(1)}]^2 \right) \right), \quad (27)$$

To make  $1 \leq BO_I \leq 2$  requires  $n_I \geq 2$ , where  $n_I$  is a real number. The bond order is not used for the triple bonds. Finally, the van der Waals energy increment,  $E_{vdW}$ , used in Eq. (22) and (23) is given by

$$E_{\text{vdW}}(R_I) = e_{\text{vdW}} \cdot \left\{ 2 \cdot \left[ \frac{r_{\text{vdW}}}{R_I} \right]^9 - 3 \cdot \left[ \frac{r_{\text{vdW}}}{R_I} \right]^6 \right\}, \quad (28)$$

where  $e_{\text{vdW}}$  is the van der Waals binding energy, and  $r_{\text{vdW}}$  is the position of the van der Waals minimum. Note that  $r_{\text{vdW}}$  in Eq. (28) is different from  $\hat{r}_{\text{vdW}}$ , the radial cutoff used in calculating the counting factors introduced earlier in this section. This equation is similar to the 9-6 potential in the work of Warshel and Lifson.<sup>15</sup> The details to get the parameters is explained in the parameterization section. We call this new formalism MEAM-BO (MEAM with Bond Order).

## 2.2 Potential parametrization

### 2.2.1 Model calibration database

In this section, we turn our attention to the parameterization for saturated and unsaturated hydrocarbons. In this work, C, H, and CH parameters were calibrated using a saturated hydrocarbon database, and the double and triple bond parameters were calibrated using an unsaturated hydrocarbon database. The experimental data and FP results used for MEAM-BO model calibration included that for various isomers and dimers, diamond properties, and dense systems of small molecules, and that of  $\text{C}_2\text{H}_2$ ,  $\text{C}_2\text{H}_4$ , benzene, graphene, and graphite for the unsaturated hydrocarbon parameters. Specifically, for the carbon parameters, the experimental data of diamond elastic constants from the work of Grimsditch and Ramdas,<sup>16</sup> the linear chain (LC), simple cubic (SC), BCC, and FCC carbon phase FP results from the work of Yin and Cohen<sup>17</sup> and Perriot *et al.*<sup>18</sup> were used. The calculation method for FP results for HCP structure was the local density approximation (LDA) with norm-conserving pseudopotential,<sup>17</sup> while the calculation method for the other carbon phases are not specified in the paper.<sup>18</sup> The calculation method for the relative energy between graphene and graphite is Quantum Monte Carlo.<sup>19</sup> For H parameters, FP results for the dissociation energy of  $\text{H}_2$  calculated in this work, the dimer interaction of  $\text{H}_2$  (four configurations),  $\text{CH}_4$  (four configurations),  $\text{C}_2\text{H}_6$  (four configurations), and  $\text{C}_3\text{H}_8$  (three configurations) from the work of Burton and Senff,<sup>20</sup> Szczesniak *et al.*,<sup>21</sup> Rowley *et al.*,<sup>22</sup> and Jalkanen *et al.*,<sup>23</sup> respectively, were used. The calculation methods are the coupled-cluster singles and doubles method with a

1 second-order perturbation correction (CCSD(2)) with the aug-cc-pVTZ basis,<sup>24,25</sup> the coupled electron pair  
2 approximation with pair natural orbitals (CEPA-PNO),<sup>26</sup> Møller-Plesset perturbation theory with the  
3 supermolecular Møller-Plesset perturbation theory (IMPPT/MPPT),<sup>27,28</sup> and second-order Møller-Plesset  
4 perturbation theory (MP2) with the 6-311+G(2df,2pd) basis<sup>29,30</sup> for the H<sub>2</sub> dissociation energy, potential energy  
5 of H<sub>2</sub> dimer, CH<sub>4</sub> dimer, and C<sub>2</sub>H<sub>6</sub>/C<sub>3</sub>H<sub>8</sub> dimers, respectively. For CH parameters, the FP results used for this  
6 work are the CH<sub>4</sub> dissociation energy calculated using CCSD(2) with the aug-cc-pVTZ basis. Also, especially  
7 for the associated screening parameters, we used the experimental data for the H-C-H angles of CH<sub>3</sub> (methyl  
8 radical). The experimental data and FP results mentioned above are particularly for certain type of the  
9 parameters. The following saturated hydrocarbon database affects all C, H, and CH parameters. Experimental  
10 data for atomization energies, bond lengths, and bond angles of the molecules in alkane group from NIST  
11 Computational Chemistry Comparison and Benchmark Database<sup>31</sup> were employed. FP results for the rotational  
12 energy barrier of C<sub>2</sub>H<sub>6</sub> were calculated using CCSD(T) with the aug-cc-pVTZ basis for this work, and fitting  
13 result from the experimental work of Herrebout *et al.*<sup>32</sup> was used for the rotational energy barrier of *n*-butane.  
14 Finally, for unsaturated hydrocarbon fitting, FP results for the dissociation energy of C<sub>2</sub>H<sub>2</sub>, C<sub>2</sub>H<sub>4</sub>, benzene, and  
15 graphene, the elastic constants of graphene, the bending energy barrier of C<sub>2</sub>H<sub>2</sub>, and the rotational energy of  
16 C<sub>2</sub>H<sub>4</sub>, as well as the experimental data for the atomization energy of graphite from the work of Brewer,<sup>33</sup> the  
17 interplane distance of graphite from the work of Zhao and Spain<sup>34</sup>, and the elastic constants of graphite from  
18 Kelly<sup>35</sup> were used. All calculations included using CCSD(2) with aug-cc-pVTZ basis except the dissociation  
19 energy and the elastic constants<sup>36</sup> of graphene, which were calculated using the Perdew-Burke-Ernzerhof (PBE)  
20 exchange correlation functional.<sup>37</sup> For accurate predictions, the zero point energy (ZPE) as calculated by the  
21 authors was considered in certain cases such as the atomization energies and dissociation energies. Finally, one  
22 experimental pressure CH<sub>4</sub> dense system with the density of 0.5534 g/cm<sup>3</sup> at 373K taken from Cristancho *et*  
23 *al.*<sup>38</sup> was used for the calibration. Table 1 shows the details of the database used for hydrocarbon  
24 parameterization. The following two subsections contain the details of the parameterization for saturated and  
25 unsaturated hydrocarbon.

Table 1

### 2.2.2 Parametrization for saturated hydrocarbon

The first task for the MEAM parameterization is fitting the reference structures by the universal equation of state (UEOS) in Eq. (8). The reference structures for C, H, and CH parameters are diamond cubic, diatomic H<sub>2</sub>, and CH<sub>4</sub>, respectively. The choice of reference structure for CH is not unique. For example, the CH diatomic molecule was used in our previous work<sup>9</sup>, and ethylene was used in Valone *et al.*'s work<sup>39</sup>.

As a first step for the parameterization, the five UEOS parameters for C, H, and CH are obtained. For this work, the  $R_C^0$ ,  $E_C^0$ ,  $\alpha_C^0$ ,  $\delta_C^a$ , and  $\delta_C^r$  and  $R_H^0$ ,  $E_H^0$ ,  $\alpha_H^0$ ,  $\delta_H^a$ , and  $\delta_H^r$  in Eq. (8) were taken from our previous work<sup>9</sup>, which were correlated with the cohesive energy, lattice constant, and bulk modulus of the diamond cubic structure.  $R_{CH}^0$ ,  $E_{CH}^0$ ,  $\alpha_{CH}^0$ ,  $\delta_{CH}^a$ , and  $\delta_{CH}^r$  were calculated using CH<sub>4</sub> energy versus C-H distance curve where all four hydrogen atoms are simultaneously and uniformly stretched in each C-H bond direction.

Next, we start by varying the remaining C parameters such as  $\beta_C^{(0-3)}$  and  $t_C^{(1-3)}$  to obtain the desired properties of the diamond cubic reference structure, such as the cohesive energy, the lattice constant, and the elastic constants. Another consideration during this carbon parameterization is to make sure that the diamond cubic structure is more stable than the other carbon phases such as FCC and BCC. FP energies of the different carbon phases relative to the diamond cubic energy are used to avoid such structures during the parameterization procedure. Therefore, parameters are sought to satisfy the energy conditions of the different phases while maintaining the diamond properties. These target properties can be checked manually by the direct grid search method and/or the fitted during the simplex optimization procedure described below. Detailed results for the carbon properties are given in Section 3.2.

After that, to fine-tune the parameters, we employ an optimization process called the downhill simplex method by Nelder and Mead,<sup>40</sup> which is a heuristic search over a nonlinear solution space to find the minimum of an objective function by evaluating the initial set of points (a simplex of  $n+1$  points for  $n$ -dimensional vectors

$\mathbf{x}$ ) and deciding which direction to proceed. With this method, we can find a solution for the problem defined as the following.

$$\mathbf{x}^* = \underset{\mathbf{x}}{\operatorname{argmin}} f(\mathbf{x}) \quad (29)$$

where  $\mathbf{x}$  is the C and CH parameters except the UEOS parameters, which are fixed during this procedure,  $\mathbf{x}^*$  is an optimal set of the parameters, and  $f(\mathbf{x})$  is objective function, defined as follows:

$$f(\mathbf{x}) = \sum_i \omega_i \cdot e_i(\mathbf{x}) \quad (30)$$

where  $\omega_i$  is a weighting constant for the target property  $i$ , e.g.,  $\omega_{\text{energy}} = 10$ ,  $\omega_{\text{C-C length}} = 200$ ,  $\omega_{\text{C-C-C angle}} = 0.07$ ,  $\omega_{\text{carbon phase}} = 0.1$ ,  $\omega_{\text{CH}_3 \text{ radical}} = 0.1$  for this work, and  $e_i(\mathbf{x})$  is decision variable which is the root mean square (RMS) error given below.

$$e_i(\mathbf{x}) = \sqrt{\frac{1}{N} \sum_j [f_{\text{MEAM}}(\mathbf{x}, j) - C_{\text{expt}}(j)]^2} \quad (31)$$

where  $f_{\text{MEAM}}(\mathbf{x}, j)$  is one output property, such as an energy or a bond length, of the MEAM calculation of the molecule  $j$  using the parameter set  $\mathbf{x}$ ;  $C_{\text{expt}}(j)$  is the experimental result of the molecule  $j$ ; and  $N$  is the number of molecules to compare. Starting with the previously obtained parameter set, the downhill simplex method tries to find an optimal parameter set that satisfies the diamond/carbon properties, hydrocarbon molecules' properties, and formation of the radicals. Table 2 shows the details of the weights and the target values with the appropriate units.

Once this initial parameterization procedure for the C and CH parameters is completed, the H parameters are adjusted by fitting the energy curves of the set of dimers ( $\text{H}_2$ ,  $\text{CH}_4$ ,  $\text{C}_2\text{H}_6$ , and  $\text{C}_3\text{H}_8$ ) as introduced in Section 2.2.1. The downhill simplex method is again used for this optimization. Because the target data are not single valued but multiple valued garnered from the energy versus distance curve per dimer molecule, the decision variables in Eq. (31) become slightly different. The weights for the energy points per dimer molecule follow a Gaussian curve so that the weight at the equilibrium distance becomes unity in which the weights gradually decrease to zero as the distance traverses away from the equilibrium distance. This

1 optimization process finds the optimal solution for sixteen dimer interactions (four configurations of (H<sub>2</sub>)<sub>2</sub>,  
2 (CH<sub>4</sub>)<sub>2</sub>, and (C<sub>2</sub>H<sub>6</sub>)<sub>2</sub>, and three configurations of (C<sub>3</sub>H<sub>8</sub>)<sub>2</sub>) while maintaining the dissociation energies of H<sub>2</sub> and  
3 CH<sub>4</sub> close to the FP results. This H parameter optimization was accompanied by a convexity check to avoid the  
4 energy curves of having a non-convex form by a misparametrization. Finally, one hydrogen parameter  $\beta_{\text{H}}^{(1)}$  is  
5 adjusted for the pressure and the density of the dense systems described in Section 3.7. The pressure of the  
6 dense systems is most sensitive to the parameter  $\beta_{\text{H}}^{(1)}$ . As mentioned in Section 2.2.1, the parameter is adjusted  
7 to match the experimental pressure CH<sub>4</sub> dense system with the density of 0.5534 g/cm<sup>3</sup> at 373 K. As a result of  
8 this process, sixteen parameters for C and H and thirteen additional parameters for CH are obtained for the  
9 saturated hydrocarbon system as listed in Table 3 and Table 4. One noticeable change in this work compared to  
10 the previous work<sup>9</sup> is that the  $C_{\text{max}}(\text{C}, \text{C}, \text{C})$  and the  $C_{\text{min}}(\text{C}, \text{C}, \text{C})$  values decreased from 2.800 to 2.064 and from  
11 2.000 to 0.830, respectively, to unscreen the 3NN interactions, which gives much a better agreement between  
12 the diamond elastic constants and experimental values than those of our previous work as discussed below in  
13 Section 3.2.

31 **Table 2**

32 **Table 3**

33 **Table 4**

### 40 2.2.3 Parametrization for unsaturated hydrocarbons

41 Because of the additive characteristic of the bond energy to the total energy, the potential  
42 parameterization for unsaturated bonds may be developed after the parameterization for saturated bonds. For  
43 the parameterization, the dissociation energies of C<sub>2</sub>H<sub>2</sub> for triple bond and C<sub>2</sub>H<sub>4</sub>, benzene, and graphene for  
44 double bond are used. The energies are calculated when one carbon atom is being stretched (C<sub>2</sub>H<sub>2</sub> and C<sub>2</sub>H<sub>4</sub>) or  
45 all carbon atoms are being stretched homogenously (benzene and graphene) while C-H bonds are fixed. The  
46 parameterization steps are the following. First, we determine the  $e_k$  parameters for the four reference structures  
47  
48  
49  
50  
51  
52  
53  
54  
55  
56  
57  
58  
59  
60

including C<sub>2</sub>H<sub>2</sub> for the triple bond and C<sub>2</sub>H<sub>4</sub>, benzene, and graphene for the double bond. Specifically, we used the following model equation to describe the additional energy due to the unsaturation.

$$E_{\text{bond}}(R_I) = \frac{E_{\text{FP}}(R_I) - E_{\text{MEAM}}(R_I)}{N_{\text{bond}}}, \quad (32)$$

where  $N_{\text{bond}}$  is the number of bonds per molecule or atom (e.g. 1 for C<sub>2</sub>H<sub>2</sub> and C<sub>2</sub>H<sub>4</sub>, 6 for benzene, and 3/2 per C atom for graphene). Here  $E_{\text{bond}}$  corrects the saturated MEAM energy  $E_{\text{MEAM}}$  to the energy from first principles/experiment  $E_{\text{FP}}$ . We note that  $E_{\text{bond}}$  becomes the target energy for each reference state to be fitted by Eq. (22) or (23). The remaining parameter  $\beta_{\text{bond}}^{(2)}$  is set to an arbitrary value (5 was used in this work), and the remaining additive energy,  $E_{\text{vdW}}$  in Eq. (22) and (23) is set to zero as an initial guess. As a result, we can obtain three  $e_k$  parameters ( $k = \{0,1,2\}$ ) per each reference structure. Next, only for a double bond the bond order dependence based on the total nine  $e_k$  parameters from the previous step are then fitted by a second order polynomial to obtain  $g_{kl}$  parameters in Eq. (25). In a similar way, the bond length increment based on the experimental bond length is fitted for  $r_l$  parameters in Eq. (24) for the double bond. Next,  $\beta_2^{(2)}$  and  $\beta_3^{(2)}$  parameters in Eq. (22) and (23) for double/triple bonds are adjusted to make the appropriate transition from unsaturated energy to saturated bonding energy. Again, as an extra step only for the double bond,  $\beta_2^{(1)}$  and  $\beta_2^{(2)}$  are adjusted to correct the graphene properties including elastic constants. Especially,  $\beta_2^{(2)}$  is responsible for the graphene properties, *i.e.* modulus and Poisson's ratio and the smoothness of the energy increment to the energy for saturated bond. Increasing  $\beta_2^{(2)}$  value would decrease the modulus/the Poisson's ratio of graphene and increase smoothness of the transition between the energy for saturated bond to unsaturated bond. On the other hand, decreasing  $\beta_2^{(2)}$  value would increase the modulus/the Poisson's ratio but make the transition rough so that it may create a bump. Therefore, one should carefully choose  $\beta_2^{(2)}$  considering this trade-off.

The aforementioned steps may be iterated for further improving the properties including the cohesive energies and the bond lengths of the unsaturated molecules and the graphene elastic constants. The van der Waals parameters,  $r_{\text{vdW}}$  and  $e_{\text{vdW}}$  in Eq. (28) are then adjusted to get the correct A-B stacking distance, the

1 formation energy, and  $C_{33}$  of graphite. Specifically, the van der Waals energy increment,  $E_{\text{vdW}}(R_I)$  in Eq. (28),  
 2 is calculated based on the relationships between the two types of C atoms in graphite; one type is an atom that is  
 3 aligned to the other atoms above and below in the normal direction of the graphene plane, and the other type is  
 4 an atom that is not aligned. The detail is shown in Figure 1.  
 5  
 6  
 7  
 8

### 9 Figure 1

10 The van der Waals energy increment is determined so that the total energy in Eq. (15) has a minimum at  
 11 the experimental c distance, and the value of the formation energy and  $C_{33}$  are close to experiment. In Eq. (15),  
 12  $f_{I3} = 0$ ,  $f_{I2} = 1$ ,  $S_{i_1 i_2} = 0$ , and the van der Waals contribution to the sum of the out-of-plane bonds is given by  
 13  
 14  
 15  
 16  
 17

$$18 \sum_I E_{\text{vdW}}(R_I) = \frac{1}{4} \cdot [2 \cdot E_{\text{vdW}}(R_{I,\text{aligned}}) + 6 \cdot E_{\text{vdW}}(R_{I,\text{non-aligned}})] \quad (33)$$

19 where  $R_{I,\text{aligned}}$  is the distance between the aligned atoms indicated as the dashed line in Figure 1, and  
 20  $R_{I,\text{non-aligned}}$  is the distance between the non-aligned atoms indicated as the solid line. Note that this long  
 21 range interaction term only affects the interplane interaction of the graphite, not the other interactions such as  
 22 dissociation and dimer interactions, where there are no long C-C bonds. Finally, the  $\beta_{\text{bond}}^{(3)}$  and  $p_{\text{bond}}^{(3)}$   
 23 parameters of the  $D(Z)$  functions in Eq. (21) are adjusted to fit the unsaturated MEAM energy to the FP results  
 24 of the  $\text{C}_2\text{H}_4$  rotational energy barrier and  $\text{C}_2\text{H}_2$  bending energy barrier. One last note is that the  $p_{\text{bond}}^{(0)}$  and  $p_{\text{bond}}^{(1)}$   
 25 parameters are held to one, because the parameters do not affect the target properties in this work. Table 5  
 26 shows the resultant nineteen parameters for double bond and ten parameters for triple bond, and Table 6 shows  
 27 the three parameters for the van der Waals terms.  
 28  
 29  
 30  
 31  
 32  
 33  
 34  
 35  
 36  
 37  
 38  
 39  
 40  
 41  
 42  
 43  
 44

### 45 Table 5

### 46 Table 6

1 The overall parametrization procedure and the associated parameters to be determined are listed in Table  
2  
3 7. A set of parameters at each step is chosen through a sensitivity analysis similar to the work of Tschopp *et*  
4  
5 *al.*<sup>41</sup> All procedures described herein were carried out using Matlab, and its built-in function `fminsearch` was  
6  
7 used for the downhill simplex method used.  
8

### 9 10 **Table 7**

## 11 **3. Results and discussion**

### 12 13 **3.1 Simulation setup**

14  
15 The MEAM, REBO, and ReaxFF calculations were performed on the open-source large scale  
16  
17 atomic/molecular massively parallel simulator (LAMMPS) software package<sup>42</sup> (version August 10, 2015), and  
18  
19 MEAM-BO calculations were performed on DYNAMO software (version 13.1.18 modified to include MEAM  
20  
21 and then MEAM-BO) developed by Foiles, Daw, and Baskes.<sup>43</sup> The REBO version compared in this work is  
22  
23 the AIREBO by Stuart *et al.*<sup>44</sup> based on the work of Brenner's REBO potential<sup>45</sup> augmented with explicit 12–6  
24  
25 dispersion terms to deal with the long range interaction and with torsional terms to describe rotational barriers.  
26  
27 The reason to choose AIREBO instead of the second generation REBO<sup>46</sup> is because the dimer interactions  
28  
29 compared in this work are only correctly handled by AIREBO. The cutoff scale for the REBO in LAMMPS  
30  
31 package was set to 3 (about 10 Å) so that it can handle long range interactions, and both long range terms and  
32  
33 torsional terms were utilized for the energy calculation. Two different versions of ReaxFF are available in  
34  
35 LAMMPS, the FORTRAN and C versions. We used the C version of ReaxFF implemented by Aktulga *et al.*<sup>47</sup>  
36  
37 The hydrocarbon parameters for ReaxFF compared in this work is the work of Chenoweth *et al.*<sup>48</sup> There are  
38  
39 other hydrocarbon parameters such as the work of Strachan *et al.*<sup>49</sup> and Mattsson *et al.*<sup>50</sup>, but only Chenoweth's  
40  
41 parameters produce the correct radicals and the correct energy curves for some of the hydrocarbon dimer  
42  
43 interactions.  
44  
45  
46  
47  
48  
49  
50

51  
52 Initial configurations for the single molecules were taken from the experimental data or the minimized first  
53  
54 principles structure in the NIST Computational Chemistry Comparison and Benchmark Database.<sup>31</sup> Initial  
55  
56 structures for the dimers were generated using the single molecules above according to the respective paper.  
57  
58  
59  
60

Initial configurations for the dense systems were generated by the BIOVIA Materials Studio software (version 5.5). For the energy optimization, the conjugate gradient method was used. To measure the accuracy of the overall results, we used the RMS error defined in Eq. (31) and mean absolute percentage (MAP) error given by

$$e = \left[ \frac{1}{N} \sum_j \left| \frac{f_{\text{MEAM}}(j) - C_{\text{expt}}(j)}{C_{\text{expt}}(j)} \right| \right] \cdot 100, \quad (34)$$

where  $f_{\text{MEAM}}(\mathbf{x}, j)$  is one output property, such as energy or bond length, of the MEAM calculation of the molecule  $j$  using the parameter set  $\mathbf{x}$ ,  $C_{\text{expt}}(j)$  is the experimental result of the molecule  $j$ , and  $N$  is the number of the molecules to compare. Finally, unless MEAM-BO is explicitly specified, MEAM and MEAM-BO are used interchangeably in this results section because both give the same results when all carbon bonds are fully saturated.

### 3.2 Carbon properties

Table 8 compares the new MEAM (MEAM-BO) results for carbon properties (cohesive energies of different crystal structures, lattice constants, and elastic constants of diamond, graphite, and graphene) with experimental data,<sup>16,33–35,51,52</sup> FP results,<sup>17,18,53</sup> the previous results<sup>9</sup> of MEAM, REBO results, and ReaxFF results. In addition to individual prediction values, RMS and MAP errors of subgroups of properties are also listed. The calculated energies of the different crystal structures are relative to the energy of the diamond cubic structure. For elastic constants calculations, a linear strain-stress relationship was assumed since the strain ( $\varepsilon$ ) was small. For graphite, the elastic constants  $C_{11}$  and  $C_{12}$  were calculated based on the uniaxial/biaxial strain state:

$$C_{11} = \frac{1}{V} \cdot \frac{\partial^2 U}{\partial \varepsilon^2} \text{ (uniaxial) and } C_{11} + C_{12} = \frac{1}{V} \cdot \frac{\partial^2 U}{\partial \varepsilon^2} \text{ (biaxial)} \quad (35)$$

where  $V$  is atomic volume, and  $U$  is strain energy. Based on these results,  $C_{66}$  was calculated using the relationship between  $C_{11}$  and  $C_{12}$ ,  $C_{66} = (C_{11} - C_{12})/2$ . Alternatively,  $C_{66}$  was directly calculated using biaxial loading in similar way in Eq. (35) where graphite was stretched in one planar direction and compressed the other planar direction with the same small  $\varepsilon$ . Further,  $C_{13}$  was calculated by the following equation,

$$\frac{1}{2} \cdot \left[ \frac{C_{11} + C_{33}}{2} - C_{13} \right] = \frac{1}{4V} \cdot \frac{\partial^2 U}{\partial \varepsilon^2} \quad (36)$$

with the strain state given by  $\varepsilon_{11} = \varepsilon$  and  $\varepsilon_{33} = -\varepsilon$ . The elastic constants for graphene were similarly obtained by replacing the volume  $V$  by the area  $A$  in the above equations. The in-plane elastic constant for graphene was calculated by the equation  $Y_{2D} = [C_{11}^2 - C_{12}^2]/C_{11}$ <sup>36</sup> and divided by the experimental graphite A-B stacking distance (3.35 Å) to match the units (GPa) of the experimental data.

### Table 8

As shown in the diamond properties, the current work shows better agreement with the experimental results than the previous MEAM<sup>9</sup> results, because the 3NN contribution provides more accurate interactions. The current MEAM-BO results are on par with those of REBO and much better than those of ReaxFF. More realistic elastic constants for ReaxFF can be obtained through MD simulations as shown in the work of Jensen *et al.*<sup>54</sup>, but the results are still much greater than the experimental values. Of the three potentials, REBO produced the closest agreement with the experimental data for the diamond structure in terms of the MAP error.

As for the energy of different crystal structures, DFT calculations show that a linear chain (LC) is energetically closest to the diamond cubic structure followed by simple cubic (SC), BCC, HCP, and FCC. In this comparison, ReaxFF outperforms MEAM and REBO by giving a similar order of the relative energies for the different crystal structures, which are close to DFT calculations. The cohesive energies of SC, BCC, HCP, and FCC structures calculated by the previous MEAM parameter set<sup>9</sup> are lower than the energy of the diamond structure, while the current MEAM parameter set gives the diamond energy lower than the energies of the different crystal structures. We note that MEAM-BO increases the energy of LC, because of its triple bond character.

While MEAM and MEAM-BO can produce the same results in saturated bond environment such as the diamond properties and carbon phases except LC, only MEAM-BO correctly predicts the graphene and the graphite properties due to the unsaturated bonds. For graphene properties, MEAM-BO, REBO, and ReaxFF potentials predict the cohesive energy and the lattice constant reasonably well. MEAM-BO and REBO show good results for other graphene properties, but the MEAM-BO results are closer to the experimental data.

1 Similar to graphene, all three potentials show close results for the cohesive energy and the lattice constants of  
2 graphite. Again, the ReaxFF elastic constants are much different from the experimental data. MEAM-BO and  
3 REBO mostly agree with the experimental data while the  $C_{44}$  calculation using the new MEAM is about sixty  
4 times larger than the experimental value, resulting in increasing overall RMS and MAP error. The bottom row  
5 of the table shows the MAP error excluding the  $C_{44}$  result. One last note is that we found that MEAM with the  
6 parameter set from the previous work<sup>9</sup> gave carbon planes in graphite that collapsed giving an inappropriate low  
7 energy, high coordinated structure.  
8  
9  
10  
11  
12  
13  
14  
15  
16  
17  
18

### 19 3.3 Single molecules

20  
21 Table 9 shows the MEAM atomization energy of select alkanes and unsaturated molecules that are  
22 compared with the experimental energy at 0 K with REBO and ReaxFF. As in Brenner's work,<sup>46</sup> the  
23 experimental energies adjusted by the zero point energies (ZPE) are targeted for parameterization to reproduce  
24 the "bottom of the well" energy at the minimum. Thus, to compare these to experimental atomization energies,  
25 the ZPE must be subtracted from the atomization energies. To make these comparisons as meaningful as  
26 possible, we chose to use reasonably high quality ZPE's, namely B3LYP/cc-pVTZ ZPE's. For clarity of  
27 presentation, we chose to add the ZPE's to the MEAM-BO and REBO energies, instead of the theoretically  
28 more satisfying but numerically equivalent subtraction of the ZPE's from the experimental data. ReaxFF, on  
29 the other hand, is calibrated to reproduce heats of formation, with the ZPE's already included within the  
30 empirical heat increment.<sup>55</sup> For ReaxFF, we adjusted the energies by calculating the differences between the  
31 empirical heat increments for carbon (8.6306 eV) and hydrogen (2.7097 eV)<sup>48</sup> and the experimental energies for  
32 carbon (7.3768 eV) and hydrogen (2.375 eV),<sup>45</sup> respectively, and then subtracted the sum of the differences of  
33 each atom type multiplied by the number of atoms in order to determine the final energy per molecule. The  
34 calculated heat increment values are listed in Table 9 in which the bold numbers represent the experimental  
35 energies and the adjusted energies. Again, the RMS and MAP errors are also listed at the table bottom.  
36  
37  
38  
39  
40  
41  
42  
43  
44  
45  
46  
47  
48  
49  
50  
51  
52  
53  
54  
55  
56

57 **Table 9**

As shown in Table 9, the RMS value for the MEAM energies of the alkane group (0.031 eV) is lower than that for REBO (0.288<sup>1</sup> eV) and that for ReaxFF (2.217<sup>2</sup> eV). For the cycloalkane group, MEAM and REBO are in better agreement with the experimental data than is ReaxFF. The results for the unsaturated molecules, acetylene, ethylene, and benzene show that the MEAM-BO formalism now has the capability to distinguish bond order, giving values as close to the experimental data as REBO does. For radicals, the MEAM overpredicts the energy of CH (Methylidyne radical) and CH<sub>2</sub> (Methylene radical) by about 3 eV. We note that REBO and ReaxFF have been parameterized to a larger database of both saturated and unsaturated hydrocarbons, and the results may vary with different data sets. Hence, the comparisons in Table 9 serve only as a guide.

Table 10 shows the average bond lengths of MEAM, REBO, ReaxFF, and the experimental data for the select molecules. Similar to the energy results, the MEAM bond lengths for the alkane group molecules are more accurate than those of REBO and ReaxFF, while REBO is slightly better in the case of the cycloalkane, and the radical bond lengths of MEAM are more erroneous. Again, MEAM-BO predicted the bond length and the bond angles of the molecules with unsaturated bonds reasonably well, but the CH bond length of benzene (1.140 Å) was predicted to be much longer than that of the experimental value (1.084Å). Table 11 shows that all three potentials predicted angles that were in similar agreement with experimental results. The current MEAM parameters fixed an issue in the CH<sub>3</sub> (methyl radical) minimization that appeared in results using the previous MEAM parameters.<sup>9</sup> The geometry of CH<sub>3</sub> after energy minimization using the previous parameters were planar and gave an average ∠H-C-H bond angle of 120°; however, the individual angles were not 120° but 143.2°, 108.4°, and 108.4°. The current work corrected the issue, and now CH<sub>3</sub> is planar, and the individual angles are 120° after energy minimization. REBO gives the same result, while ReaxFF formed slightly smaller ∠H-C-H angles of 119.39° (non-planar). As a visual comparison, Figure 2 shows the differences between the

<sup>1</sup> The change from 2<sup>nd</sup> generation REBO in our previous work<sup>9</sup> to AIREBO led a small difference in the results.

<sup>2</sup> The change from the parameters by Mattsson *et al.*<sup>50</sup> in our previous work<sup>9</sup> to the parameters by Chenoweth *et al.*<sup>48</sup> led a small difference in the results.

1 new MEAM calculation of the atomization energies, the bond lengths, and the bond angles and those of the  
2 experimental data.  
3

4  
5 **Table 10**

6  
7 **Table 11**

8  
9 **Figure 2**

10  
11 Next, we performed an oversaturation test where one and two hydrogen atoms were inserted near the methane  
12 molecule as shown in the Figure 3 to check whether hydrogen atom(s) would correctly eject after energy  
13 minimization.  
14  
15

16  
17  
18 **Figure 3**

19  
20 In both tests, MEAM and ReaxFF successfully ejected the hydrogen atoms from the methane, while REBO  
21 formed a trigonal bipyramidal shape instead.  
22  
23  
24

### 25 26 27 **3.4 Bond dissociation energy**

28  
29 The bond dissociation energies of a hydrogen molecule, methane molecule, and ethane molecule calculated  
30 by the new MEAM, REBO, ReaxFF, FP, and experimental data are presented in Figure 4. As mentioned in  
31 Section 2.2.1, Figure 4(a) and (c) show the FP results from CCSD(2) and the aug-cc-pVTZ basis set  
32 calculations. Figure 4 (c) and (d) show the results of B3LYP XC functional with the 6-31G\*\* basis set<sup>56,57</sup>  
33 from the work of Lorant *et al.*<sup>58</sup>  
34  
35  
36  
37  
38  
39  
40  
41

42 **Figure 4**

43 Figure 4 shows the dissociation energy curve of (a) a hydrogen molecule, (b) a methane molecule where all  
44 hydrogen atoms are homogeneously deformed, (c) a methane molecule where only one C-H bond distance is  
45 varied, and (d) an ethane molecule where the C-C bond distance is varied at a constant C-H bond length. The  
46 energy curves of FP and ReaxFF shown in Figure 4(c) and (d) are appropriately adjusted with respect to the  
47 experimental data points so as to compare the curvature of the energy curve around the equilibration distance.  
48  
49 As mentioned in Section 2.2.2, the dissociation energy curves for hydrogen and methane molecule shown in  
50 Figure 4(a) and (b) were used for the parameterization of hydrogen and hydrocarbon parameters, respectively.  
51  
52  
53  
54  
55  
56  
57  
58  
59  
60

Therefore, the new MEAM calculations gave results very close to the experimental results. The positive energies for the FP curve after 2.5 Å shown in Figure 4(b) are due to the carbon atom going to the incorrect electronic state as all four bonds are simultaneously broken. For H<sub>2</sub>, the REBO and Reaxff results both disagree with the FP results at bond lengths 1.5-3 Å, while by construction, the new MEAM agrees well. Near equilibrium all potentials perform acceptably well. For the other three tests, the new MEAM calculated energy curves follow the FP energy curve near the equilibrium distance as do REBO and ReaxFF. Because new MEAM overpredicts the energy of the CH<sub>3</sub> radical as summarized in Table 9, the new MEAM energy (see Figure 4(c) and (d)) is lower at full dissociation than those of FP and the other potentials.

Figure 5 compares the bond dissociation energies of acetylene, ethylene, benzene, and graphene calculated using the MEAM-BO, REBO, ReaxFF, FP, and experimental data. For acetylene, ethylene, and benzene, the geometries were from CCSD(T)/aug-cc-pVTZ calculations, while the energies are CCSD(2)/aug-cc-pVTZ calculations. For graphene, the calculation was performed using a PBE exchange correlation functional with the RRKJ pseudopotential<sup>37,59</sup> as mentioned in Section 2.2.1. Similar to the homogeneous expansion of methane in Figure 4(b), all atoms of the benzene and the graphene were homogeneously deformed while calculating the energies. Also, the FP results were appropriately adjusted so that the equilibrium energy and the corresponding distance match the experimental data in order to compare the curvature of the energy.

### Figure 5

As all of these molecules shown in Figure 5 are used in the fitting process introduced in Section 2.2.3, the energy calculation results by MEAM are well matched to the FP calculation results around the equilibrium distance. REBO also shows good predictions, but ReaxFF predicts the energy a few eV lower than the FP calculations. This is understandable because ReaxFF parameters were not derived from the cohesive energy but the dissociation energy and heat of formation.

### 3.5 Dimer molecules

In this section, the energies of four different dimers (hydrogen, methane, ethane, and propane) were calculated as a function of molecular separation for various relative orientations. FP results for the hydrogen

1 dimer interaction were taken from the work of Burton *et al.*,<sup>20</sup> who used the CEPA-PNO<sup>26</sup> method. Four  
2 different configurations, collinear coplanar (T shape), linear, parallel, and crossed were chosen. Figure 6 shows  
3 a comparison of MEAM, REBO, and ReaxFF results with the FP results, and the details of the configuration are  
4 depicted on the top of each sub-figure. The energy was calculated as a function of relative displacement of two  
5 rigid molecules and adjusted by the total energy of the structure at an infinite atomic distance. The FP results  
6 for methane, ethane, and propane dimer interactions were taken from the work of Szczesniak *et al.*,<sup>21</sup> Rowley *et*  
7 *al.*,<sup>22</sup> and Jalkanen *et al.*.<sup>23</sup> The FP simulations employed the IMPPT/MPPT<sup>27,28</sup> methods for the methane dimer  
8 and MP2/6-311+ G(2df,2pd)<sup>29,30</sup> for the ethane and propane dimers. Similar to the hydrogen dimer results, all  
9 methane, ethane, and propane dimer interaction results calculated by MEAM, REBO, and ReaxFF are compared  
10 with the associated FP results in the Figure 7, Figure 8, and Figure 9, respectively. The arrows and the dashed  
11 lines in the detail on the top of each sub-figure indicate the distance that was varied. For all dimer interaction  
12 results in this work, the distances were measured between the nearest carbon atoms (or hydrogen atoms in  
13 hydrogen dimers). For consistency, the original FP results were shifted according to the distance measure used  
14 in this work.

15  
16  
17  
18  
19  
20  
21  
22  
23  
24  
25  
26  
27  
28  
29  
30  
31  
32  
33 A few observations can be asserted by viewing Figures 6-9. First, the ReaxFF results are very close to the  
34 FP results, especially the collinear coplanar and parallel configurations of the hydrogen dimer and the F  
35 configuration of the methane dimer shown in Figure 6(a) and (b), and Figure 7(d), respectively. Second, for the  
36 hydrogen dimers, the energy curves of REBO and ReaxFF around the equilibrium distance are well aligned  
37 with the FP results, although they disagree beyond the equilibrium distance where the molecules repel each  
38 other. Third, the equilibrium distances of the dimers calculated by ReaxFF overall are shorter than those of the  
39 MEAM, REBO, and FP calculations. Fourth, MEAM calculations consistently overpredict the dimer bonding  
40 compared to the FP results. A part of the reason for the lower minimum energy is that one of the hydrogen  
41 parameters,  $\beta_{\text{H}}^{(1)}$ , used for the pressure correction of the dense molecular systems described in Section 2.2.2,  
42 changes the energy curvature and lowers the energy of the dimer interactions. We considered the pressure-  
43 volume-temperature (PVT) relationship in the dense molecular systems more important than the curvature of  
44  
45  
46  
47  
48  
49  
50  
51  
52  
53  
54  
55  
56  
57  
58  
59  
60

1 the dimer interactions. Also, note that there is no explicit van der Waals term in the MEAM formalism<sup>3</sup> to  
2 correctly handle the long range interactions. As mentioned earlier, even though the MEAM-BO formalism  
3 includes the 9-6 long range interaction term, it is only implemented for long unsaturated C-C bonds. The van  
4 der Waals interactions are expressed in the exponential tails of the MEAM potential, which will be addressed  
5 further in a future work.  
6  
7  
8  
9  
10

11 **Figure 6**

12 **Figure 7**

13 **Figure 8**

14 **Figure 9**

### 15 **3.6 Rotational/bending barrier**

16 In this section, we calculated the rotational/bending barrier using the saturated molecules ethane and *n*-  
17 butane, and the unsaturated molecules acetylene and ethylene. The rotation simulation setup was that the  
18 energies were calculated at angles where a subset of the atoms of the energy minimized structure were rotated  
19 while the other atoms were only allowed to move along the axis parallel to the C-C bond (the middle C-C bond  
20 for *n*-butane). For ethane, three hydrogen atoms were rotated about the axis along the C-C bond, and for *n*-  
21 butane three hydrogen atoms and the nearest carbon atom were rotated about the axis along the middle C-C  
22 bond. The calculation method for ethane was CCSD(2) with aug-cc-pVTZ basis.<sup>24,25</sup> For *n*-butane, the data fit  
23 came from the experimental work of Herrebout *et al.*<sup>59</sup> Figure 10 shows the rotational barriers for ethane and *n*-  
24 butane calculated by MEAM, REBO, ReaxFF; the associated FP results for ethane, and experimental data fit for  
25 *n*-butane.  
26  
27  
28  
29  
30  
31  
32  
33  
34  
35  
36  
37  
38  
39  
40  
41  
42  
43  
44  
45

46 **Figure 10**

47 As shown in Figure 10, the rotational barriers calculated using MEAM and REBO for ethane are close to the FP  
48 results, while that for ReaxFF is a bit higher. For *n*-butane the previous work<sup>9</sup> had dips in the energy curve that  
49 gave three different minimum energy structures at the angles of 120°, 180°, and 240°, resulting in an incorrect  
50  
51  
52  
53  
54  
55

---

56  
57 <sup>3</sup> van der Waals term is added to MEAM-BO to correct the graphite energy, but this does not affect dimer interactions.  
58  
59  
60

1 angular distribution in MD simulations of a polyethylene system. The current work shows only one  
2  
3 minimum energy at  $180^\circ$ , the same as the experimental results, REBO, and ReaxFF calculations. However,  
4  
5  
6 the peaks of the rotational barriers at  $120^\circ$  and  $240^\circ$  calculated using MEAM for *n*-butane are lower than the  
7  
8  
9 experimental data fit by 0.08 eV. The barrier from REBO is in excellent agreement with the experimental data  
10  
11  
12 fit at dihedral angle from  $80^\circ$  to  $280^\circ$  while the barrier from MEAM is in good agreement at dihedral angle from  
13  
14  
15  
16  $0^\circ$  to  $60^\circ$  and from  $300^\circ$  to  $360^\circ$ , and the barrier from ReaxFF is between that of MEAM and REBO.  
17  
18

19 Next, the bending energy barrier of acetylene and the rotational energy barrier of ethylene are presented  
20  
21 in Figure 11. For bending energy barrier of acetylene, the coordinates were varied while keeping C-H bond  
22  
23 distance the same. Unlike the tests for other molecules, the initial structures of ethylene for various dihedral  
24  
25 angles were constructed in such a way that the C-C bond distance is set to the distance calculated by FP at each  
26  
27 angle because the bond order of ethylene is changed from a double bond to a single bond as the angle changes.  
28  
29 C-H bond length was kept the same. After that, the energy was obtained under the constrained minimization  
30  
31 described above; all atoms are allowed to move along the axis parallel to the C-C bond.  
32  
33  
34  
35

### 36 Figure 11

37  
38 As shown in Figure 11 for acetylene, both MEAM-BO and REBO agree with the FP results near the  
39  
40 equilibrium angle, but ReaxFF gives a significantly stiffer response. Also, MEAM-BO and ReaxFF do not  
41  
42 capture the energy barrier as the bending angle increase while REBO captures the trend well. Similarly for  
43  
44 ethylene, both MEAM-BO and ReaxFF agree with the FP results near equilibrium and predict a significantly  
45  
46 lower barrier than FP as the angle become a right angle. On the contrary, REBO gives stiffer behavior near the  
47  
48 equilibrium and gives a barrier closer to the FP results around  $90^\circ$ . The barrier from MEAM-BO is  
49  
50 underestimated because the predicted energy of twisted  $C_2H_4$  is too low. We tried to raise this energy but were  
51  
52 not able to do so without significantly changing other properties.  
53  
54  
55

### 56 3.7 Molecular dynamics (MD) simulations

1 In this section the results of MD calculations for select alkane systems are compared with experimental  
2 pressure-volume-temperature (PVT) data. A series of MD simulations were run with NVT (constant number of  
3 atoms  $N$ , constant volume  $V$ , and constant temperature  $T$ ) on a series of 3D periodic methane, ethane, propane,  
4 and butane systems with different densities and at different temperatures (Table 12). As shown in our previous  
5 work,<sup>9</sup> the cut-off radius was kept as 5 Å, because the difference between the results with the cut-off radius 5 Å  
6 and those of the radius longer than 5 Å was marginal.<sup>9</sup> We built the starting periodic structures using Materials  
7 Studio and ran the MD simulations using LAMMPS for a total simulation time of 400 ps with a time step of 0.4  
8 fs. A typical run time was 2-12 hours on 24 cores depending on the number of molecules and the density of the  
9 system. A Nose-Hoover thermostat was used to control the temperature. The damping factor for thermostat  
10 was 1 fs. All systems equilibrated after 300 ps. The calculated pressures for each time step were time-averaged  
11 over the last 100 ps of the simulation, and an average pressure was calculated. The details of dynamics  
12 simulations and the final average pressures of MEAM, REBO, ReaxFF, and the experimental data are given in  
13 Table 12. As shown in Table 12, the RMS (MAP) errors for MEAM, REBO, and ReaxFF are 34.8 MPa  
14 (59.2%), 173.9 MPa (246.2%), and 183.4 MPa (907.2%), respectively.

15  
16  
17  
18  
19  
20  
21  
22  
23  
24  
25  
26  
27  
28  
29  
30  
31  
32  
33 Finally, we performed an NPT (constant number of atoms  $N$ , constant pressure  $P$ , and constant temperature  
34  $T$ ) simulation for an amorphous polyethylene system with 20 chains of 250 monomers (30,040 atoms).  
35 Amorphous polyethylene of the initial density of 0.85 g/cm<sup>3</sup> as the same as the theoretical density was  
36 generated by Materials Studio, the energy minimization using COMPASS potential<sup>60</sup> was carried out, and an  
37 MD simulation with a Nose-Hoover thermostat was performed for 400 ps after the energy minimization. The  
38 damping factor for the thermostat and the barostat were 1 fs and 8 fs, respectively. The results of the final 100  
39 ps were averaged. The final averaged density from MEAM, REBO, ReaxFF, and COMPASS was 0.804 g/cm<sup>3</sup>,  
40 0.717 g/cm<sup>3</sup>, 0.964 g/cm<sup>3</sup>, and 0.832 g/cm<sup>3</sup>, respectively. Figure 12 (a) shows MEAM, REBO, ReaxFF, and  
41 COMPASS calculations of the density changes over time during the NPT simulation, and Figure 12 (b) shows  
42 the C-C-C-C dihedral angle distributions of the geometries at the last time step. The dihedral angle distribution  
43 shows the inverse trends of the rotational barrier of *n*-butane shown in Figure 10 (b), and REBO and  
44  
45  
46  
47  
48  
49  
50  
51  
52  
53  
54  
55  
56  
57  
58  
59  
60

1 COMPASS show much lower distribution at 120° and 240° than MEAM and ReaxFF due to the higher energy  
2  
3  
4 barrier shown in the *n*-Butane energy curve. In terms of computational times, for the MD simulations, on  
5  
6 average MEAM is 30% slower than REBO and 6.7 times faster than ReaxFF.  
7

#### 8 **Table 12**

#### 9 **Figure 12**

### 10 **4. Summary**

11  
12  
13 A new formalism for bond order (MEAM-BO) has been added to the existing MEAM formalism to handle  
14  
15 unsaturated bonds in hydrocarbons. Before adding the bond order terms, 3NN interactions were incorporated  
16  
17 into the C diamond cubic reference state, enabling more accurate predictions of diamond cubic properties. The  
18  
19 potential optimization for saturated bonds and unsaturated bonds were consecutively performed with reference  
20  
21 to a modest database of atomization energies, bond distances, and bond angles of select molecules, the potential  
22  
23 energy curves of H<sub>2</sub>, CH<sub>4</sub>, C<sub>2</sub>H<sub>2</sub>, C<sub>2</sub>H<sub>4</sub>, benzene, graphene, (H<sub>2</sub>)<sub>2</sub>, (CH<sub>4</sub>)<sub>2</sub>, (C<sub>2</sub>H<sub>6</sub>)<sub>2</sub>, and (C<sub>3</sub>H<sub>8</sub>)<sub>2</sub>, diamond  
24  
25 properties/energies of the different carbon phases, and the pressure-volume-temperature (PVT) relationship of  
26  
27 dense molecular systems. These properties calculated using the new MEAM potential (without bond order)  
28  
29 were compared with the associated experimental data, first principles calculations, the previous MEAM  
30  
31 potential, and two other reactive potentials, REBO and ReaxFF. The current MEAM potential (without bond  
32  
33 order) successfully addresses a critical issue from the previous hydrocarbon MEAM potential, *i.e.*, diamond  
34  
35 cubic C not being the lowest energy crystal structure. For the MEAM-BO, the results also show that the  
36  
37 properties of saturated and unsaturated hydrocarbons are comparable to those of the other reactive potentials  
38  
39 and are reasonably close to the experimental data/first principles calculations. The new MEAM-BO potential  
40  
41 can easily be combined with literature MEAM potentials for many other elements, enabling computation of  
42  
43 properties of a wide variety of multi-component systems.  
44  
45  
46  
47  
48  
49  
50  
51

### 52 **Acknowledgments**

The authors would like to thank the Center for Advanced Vehicular Systems (CAVS) at Mississippi State University for supporting this work. Effort sponsored by the Engineer Research & Development Center under Cooperative Agreement number W912HZ-13-C-0037 and W912HZ-15-2-0004. The views and conclusions contained herein are those of the authors and should not be interpreted as necessarily representing the official policies or endorsements, either expressed or implied, of the Engineer Research & Development Center of the U.S. government.

## References

- (1) Alleman, C.; Srivastava, A.; Ghosh, S. Molecular Dynamics Simulations of the Effects of Carbon Dioxide on the Interfacial Bonding of Polystyrene Thin Films. *J. Polym. Sci. Part B Polym. Phys.* **2011**, *49* (16), 1183–1194.
- (2) Wang, Z.; Lv, Q.; Chen, S.; Li, C.; Sun, S.; Hu, S. Effect of Interfacial Bonding on Interphase Properties in SiO<sub>2</sub>/Epoxy Nanocomposite: A Molecular Dynamics Simulation Study. *ACS Appl. Mater. Interfaces* **2016**, *8* (11), 7499–7508.
- (3) Rissanou, A. N.; Harmandaris, V. Dynamics of Various Polymer–graphene Interfacial Systems through Atomistic Molecular Dynamics Simulations. *Soft Matter* **2014**, *10* (16), 2876–2888.
- (4) Haghghatpanah, S.; Bohlén, M.; Bolton, K. Molecular Level Computational Studies of Polyethylene and Polyacrylonitrile Composites Containing Single Walled Carbon Nanotubes: Effect of Carboxylic Acid Functionalization on Nanotube-Polymer Interfacial Properties. *Front. Chem.* **2014**, *2*.
- (5) Milano, G.; Santangelo, G.; Ragone, F.; Cavallo, L.; Di Matteo, A. Gold Nanoparticle/Polymer Interfaces: All Atom Structures from Molecular Dynamics Simulations. *J. Phys. Chem. C* **2011**, *115* (31), 15154–15163.
- (6) Semino, R.; Ramsahye, N. A.; Ghoufi, A.; Maurin, G. Microscopic Model of the Metal–Organic Framework/Polymer Interface: A First Step toward Understanding the Compatibility in Mixed Matrix Membranes. *ACS Appl. Mater. Interfaces* **2016**, *8* (1), 809–819.
- (7) Baskes, M. I.; Nelson, J. S.; Wright, A. F. Semiempirical Modified Embedded-Atom Potentials for Silicon and Germanium. *Phys. Rev. B* **1989**, *40* (9), 6085–6100.
- (8) Foiles, S. M.; Baskes, M. I.; Daw, M. S. Embedded-Atom-Method Functions for the Fcc Metals Cu, Ag, Au, Ni, Pd, Pt, and Their Alloys. *Phys. Rev. B* **1986**, *33* (12), 7983–7991.
- (9) Nouranian, S.; Tschopp, M. A.; Gwaltney, S. R.; Baskes, M. I.; Horstemeyer, M. F. An Interatomic Potential for Saturated Hydrocarbons Based on the Modified Embedded-Atom Method. *Phys. Chem. Chem. Phys.* **2014**, *16* (13), 6233.
- (10) Lee, B.-J.; Baskes, M. I.; Kim, H.; Cho, Y. Second Nearest-Neighbor Modified Embedded Atom Method Potentials for Bcc Transition Metals. *Phys. Rev. B* **2001**, *64* (18), 184102.
- (11) Baskes, M. I. Modified Embedded-Atom Potentials for Cubic Materials and Impurities. *Phys. Rev. B* **1992**, *46* (5), 2727–2742.
- (12) Daw, M. S.; Baskes, M. I. Embedded-Atom Method: Derivation and Application to Impurities, Surfaces, and Other Defects in Metals. *Phys. Rev. B* **1984**, *29* (12), 6443–6453.
- (13) Vinet, P.; Smith, J. R.; Ferrante, J.; Rose, J. H. Temperature Effects on the Universal Equation of State of Solids. *Phys. Rev. B* **1987**, *35* (4), 1945–1953.
- (14) Lee, B.-J.; Baskes, M. I.; Kim, H.; Cho, Y. Second Nearest-Neighbor Modified Embedded Atom Method Potentials for Bcc Transition Metals. *Phys. Rev. B* **2001**, *64* (18), 184102.

- 1  
2  
3  
4  
5  
6  
7  
8  
9  
10  
11  
12  
13  
14  
15  
16  
17  
18  
19  
20  
21  
22  
23  
24  
25  
26  
27  
28  
29  
30  
31  
32  
33  
34  
35  
36  
37  
38  
39  
40  
41  
42  
43  
44  
45  
46  
47  
48  
49  
50  
51  
52  
53  
54  
55  
56  
57  
58  
59  
60
- (15) Warshel, A.; Lifson, S. Consistent Force Field Calculations. II. Crystal Structures, Sublimation Energies, Molecular and Lattice Vibrations, Molecular Conformations, and Enthalpies of Alkanes. *J. Chem. Phys.* **1970**, *53* (2), 582–594.
  - (16) Grimsditch, M. H.; Ramdas, A. K. Brillouin Scattering in Diamond. *Phys. Rev. B* **1975**, *11* (8), 3139–3148.
  - (17) Yin, M. T.; Cohen, M. L. Will Diamond Transform under Megabar Pressures? *Phys. Rev. Lett.* **1983**, *50* (25), 2006–2009.
  - (18) Perriot, R.; Gu, X.; Lin, Y.; Zhakhovsky, V. V.; Oleynik, I. I. Screened Environment-Dependent Reactive Empirical Bond-Order Potential for Atomistic Simulations of Carbon Materials. *Phys. Rev. B* **2013**, *88* (6), 64101.
  - (19) Foulkes, W. M. C.; Mitas, L.; Needs, R. J.; Rajagopal, G. Quantum Monte Carlo Simulations of Solids. *Rev. Mod. Phys.* **2001**, *73* (1), 33–83.
  - (20) Burton, P. G.; Senff, U. E. The (H<sub>2</sub>)<sub>2</sub> Potential Surface and the Interaction between Hydrogen Molecules at Low Temperatures. *J. Chem. Phys.* **1982**, *76* (12), 6073–6087.
  - (21) Szczesniak, M.; Chalansinski, G.; Cybulski, S.; Scheiner, S. Intermolecular Potential of the Methane Dimer and Trimer. *J. Chem. Phys.* **1990**, *93*, 4243–4253.
  - (22) Rowley, R. L.; Yang, Y.; Pakkanen, T. A. Determination of an Ethane Intermolecular Potential Model for Use in Molecular Simulations from Ab Initio Calculations. *J. Chem. Phys.* **2001**, *114* (14), 6058–6067.
  - (23) Jalkanen, J.-P.; Mahlanen, R.; Pakkanen, T. A.; Rowley, R. L. Ab Initio Potential Energy Surfaces of the Propane Dimer. *J. Chem. Phys.* **2002**, *116* (4), 1303–1312.
  - (24) Gwaltney, S. R.; Head-Gordon, M. A Second-Order Perturbative Correction to the Coupled-Cluster Singles and Doubles Method: CCSD(2). *J. Chem. Phys.* **2001**, *115* (5), 2014–2021.
  - (25) Kendall, R. A.; Dunning, T. H., Jr.; Harrison, R. J. Electron Affinities of the First-Row Atoms Revisited. Systematic Basis Sets and Wave Functions. *J. Chem. Phys.* **1992**, *96* (9), 6796–6806.
  - (26) Ahlrichs, R.; Lischka, H.; Staemmler, V.; Kutzelnigg, W. PNO–CI (Pair Natural Orbital Configuration Interaction) and CEPA–PNO (Coupled Electron Pair Approximation with Pair Natural Orbitals) Calculations of Molecular Systems. I. Outline of the Method for Closed-Shell States. *J. Chem. Phys.* **1975**, *62* (4), 1225–1234.
  - (27) Szalewicz, K.; Jeziorski, B. Symmetry-Adapted Double-Perturbation Analysis of Intramolecular Correlation Effects in Weak Intermolecular Interactions. *Mol. Phys.* **1979**, *38* (1), 191–208.
  - (28) Pople, J. A.; Binkley, J. S.; Seeger, R. Theoretical Models Incorporating Electron Correlation. *Int. J. Quantum Chem.* **1976**, *10* (S10), 1–19.
  - (29) Head-Gordon, M.; Pople, J. A.; Frisch, M. J. MP2 Energy Evaluation by Direct Methods. *Chem. Phys. Lett.* **1988**, *153* (6), 503–506.
  - (30) McLean, A. D.; Chandler, G. S. Contracted Gaussian Basis Sets for Molecular Calculations. I. Second Row Atoms, Z=11–18. *J. Chem. Phys.* **1980**, *72* (10), 5639–5648.
  - (31) *NIST Computational Chemistry Comparison and Benchmark Database*, NIST Standard Reference Database Number 101, Release 17b, Editor: Russell D. Johnson III, September 2015, <http://cccbdb.nist.gov/>.
  - (32) Herrebout, W. A.; van der Veken, B. J.; Wang, A.; Durig, J. R. Enthalpy Difference between Conformers of N-Butane and the Potential Function Governing Conformational Interchange. *J. Phys. Chem.* **1995**, *99* (2), 578–585.
  - (33) Brewer, L. The Cohesive Energies of the Elements. *LBL-3720 Berkeley Calif.* **1977**.
  - (34) Zhao, Y. X.; Spain, I. L. X-Ray Diffraction Data for Graphite to 20 GPa. *Phys. Rev. B* **1989**, *40* (2), 993–997.
  - (35) Kelly, B. T. *Physics of Graphite*; Applied Science: London, Englewood, N.J, 1981.
  - (36) Wei, X.; Fragneaud, B.; Marianetti, C. A.; Kysar, J. W. Nonlinear Elastic Behavior of Graphene: Ab Initio Calculations to Continuum Description. *Phys. Rev. B* **2009**, *80* (20), 205407.
  - (37) Perdew, J. P.; Burke, K.; Ernzerhof, M. Generalized Gradient Approximation Made Simple. *Phys. Rev. Lett.* **1996**, *77* (18), 3865–3868.

- (38) Cristancho, D. E.; Mantilla, I. D.; Ejaz, S.; Hall, K. R.; Atilhan, M.; Iglesia-Silva, G. A. Accurate PpT Data for Methane from (300 to 450) K up to 180 MPa. *J. Chem. Eng. Data* **2010**, *55* (2), 826–829.
- (39) Valone, S. M.; Kapila, V. Nonequilibrium Atomistic Polymer Simulations under Shear and Shock Loading. In *AIP Conference Proceedings*; AIP Publishing, 2006; Vol. 845, pp 425–428.
- (40) Nelder, J. A.; Mead, R. A Simplex Method for Function Minimization. *Comput. J.* **1965**, *7* (4), 308–313.
- (41) Tschopp, M. A.; Rinderspacher, C.; Nouranian, S.; Baskes, M. I.; Gwaltney, S. R.; Horstemeyer, M. F. Quantifying Parameter Sensitivity and Uncertainty of a Reactive Interatomic Potential for Saturated Hydrocarbons. *ASCE-ASME J. Risk Uncertain. Eng. Syst. in review*.
- (42) Plimpton, S. Fast Parallel Algorithms for Short-Range Molecular Dynamics. *J. Comput. Phys.* **1995**, *117* (1), 1–19.
- (43) Foiles, S. M.; Daw, M. S.; Baskes, M. I. *DYNAMO Code*; Sandia National Laboratories, 1994.
- (44) Stuart, S. J.; Tutein, A. B.; Harrison, J. A. A Reactive Potential for Hydrocarbons with Intermolecular Interactions. *J. Chem. Phys.* **2000**, *112* (14), 6472–6486.
- (45) Brenner, D. W. Empirical Potential for Hydrocarbons for Use in Simulating the Chemical Vapor Deposition of Diamond Films. *Phys. Rev. B* **1990**, *42* (15), 9458–9471.
- (46) Brenner, D. W.; Shenderova, O. A.; Harrison, J. A.; Stuart, S. J.; Ni, B.; Sinnott, S. B. A Second-Generation Reactive Empirical Bond Order (REBO) Potential Energy Expression for Hydrocarbons. *J. Phys. Condens. Matter* **2002**, *14* (4), 783.
- (47) Aktulga, H. M.; Fogarty, J. C.; Pandit, S. A.; Grama, A. Y. Parallel Reactive Molecular Dynamics: Numerical Methods and Algorithmic Techniques. *Parallel Comput* **2012**, *38* (4–5), 245–259.
- (48) Chenoweth, K.; van Duin, A. C. T.; Goddard, W. A. ReaxFF Reactive Force Field for Molecular Dynamics Simulations of Hydrocarbon Oxidation. *J. Phys. Chem. A* **2008**, *112* (5), 1040–1053.
- (49) Strachan, A.; van Duin, A. C. T.; Chakraborty, D.; Dasgupta, S.; Goddard, W. A. Shock Waves in High-Energy Materials: The Initial Chemical Events in Nitramine RDX. *Phys. Rev. Lett.* **2003**, *91* (9), 98301.
- (50) Mattsson, T. R.; Lane, J. M. D.; Cochran, K. R.; Desjarlais, M. P.; Aidan P. Thompson; Pierce, F.; Grest, G. S. First-Principles and Classical Molecular Dynamics Simulation of Shocked Polymers. *Phys. Rev. B* **2010**, *81* (5), 54103.
- (51) Lee, C.; Wei, X.; Kysar, J. W.; Hone, J. Measurement of the Elastic Properties and Intrinsic Strength of Monolayer Graphene. *Science* **2008**, *321* (5887), 385–388.
- (52) Lee, J.-U.; Yoon, D.; Cheong, H. Estimation of Young's Modulus of Graphene by Raman Spectroscopy. *Nano Lett.* **2012**, *12* (9), 4444–4448.
- (53) Mounet, N.; Marzari, N. First-Principles Determination of the Structural, Vibrational and Thermodynamic Properties of Diamond, Graphite, and Derivatives. *Phys. Rev. B* **2005**, *71* (20), 205214.
- (54) Jensen, B. D.; Wise, K. E.; Odegard, G. M. Simulation of the Elastic and Ultimate Tensile Properties of Diamond, Graphene, Carbon Nanotubes, and Amorphous Carbon Using a Revised ReaxFF Parametrization. *J. Phys. Chem. A* **2015**, *119* (37), 9710–9721.
- (55) van Duin, A. C. T.; Dasgupta, S.; Lorant, F.; Goddard, W. A. ReaxFF: A Reactive Force Field for Hydrocarbons. *J. Phys. Chem. A* **2001**, *105* (41), 9396–9409.
- (56) Devlin, F. J.; Finley, J. W.; Stephens, P. J.; Frisch, M. J. Ab Initio Calculation of Vibrational Absorption and Circular Dichroism Spectra Using Density Functional Force Fields: A Comparison of Local, Nonlocal, and Hybrid Density Functionals. *J. Phys. Chem.* **1995**, *99* (46), 16883–16902.
- (57) Petersson, G. A.; Al-Laham, M. A. A Complete Basis Set Model Chemistry. II. Open-shell Systems and the Total Energies of the First-row Atoms. *J. Chem. Phys.* **1991**, *94* (9), 6081–6090.
- (58) Lorant, F.; Behar, F.; Goddard, W. A.; Tang, Y. Ab Initio Investigation of Ethane Dissociation Using Generalized Transition State Theory. *J. Phys. Chem. A* **2001**, *105* (33), 7896–7904.
- (59) Rappe, A. M.; Rabe, K. M.; Kaxiras, E.; Joannopoulos, J. D. Optimized Pseudopotentials. *Phys. Rev. B* **1990**, *41* (2), 1227–1230.
- (60) Sun, H. COMPASS: An Ab Initio Force-Field Optimized for Condensed-Phase Applications Overview with Details on Alkane and Benzene Compounds. *J. Phys. Chem. B* **1998**, *102* (38), 7338–7364.

- 1 (61) Hamann, D. R.; Schlüter, M.; Chiang, C. Norm-Conserving Pseudopotentials. *Phys. Rev. Lett.* **1979**, *43*  
2 (20), 1494–1497.
- 3 (62) Al-Jishi, R.; Dresselhaus, G. Lattice-Dynamical Model for Graphite. *Phys. Rev. B* **1982**, *26* (8), 4514–  
4 4522.
- 5 (63) Hasegawa, M.; Nishidate, K. Semiempirical Approach to the Energetics of Interlayer Binding in  
6 Graphite. *Phys. Rev. B* **2004**, *70* (20), 205431.
- 7 (64) Schimka, L.; Harl, J.; Kresse, G. Improved Hybrid Functional for Solids: The HSEsol Functional. *J.*  
8 *Chem. Phys.* **2011**, *134* (2), 24116.
- 9 (65) Shin, H.; Kang, S.; Koo, J.; Lee, H.; Kim, J.; Kwon, Y. Cohesion Energetics of Carbon Allotropes:  
10 Quantum Monte Carlo Study. *J. Chem. Phys.* **2014**, *140* (11), 114702.
- 11 (66) Robertson, S. L.; Babb, S. E. J. PVT Properties of Methane and Propene to 10 Kbar and 200° C. *J. Chem.*  
12 *Phys.* **1969**, *51* (4), 1357–1361.
- 13 (67) Straty, G.; Tsumura, R. PVT and Vapor Pressure Measurements on Ethane. *J Res Nbs Phys Ch* **1976**, *80*,  
14 35–39.
- 15 (68) Straty, G.; Palavra, A. Automated High Temperature PVT Apparatus with Data for Propane. *J Res Natl*  
16 *Bur Stand* **1984**, *89* (5), 375–383.
- 17 (69) Kayukawa, Y.; Hasumoto, M.; Kano, Y.; Watanabe, K. Liquid-Phase Thermodynamic Properties for  
18 Propane (1), N-Butane (2), and Isobutane (3). *J. Chem. Eng. Data* **2005**, *50* (2), 556–564.
- 19  
20  
21  
22  
23  
24  
25  
26  
27  
28  
29  
30  
31  
32  
33  
34  
35  
36  
37  
38  
39  
40  
41  
42  
43  
44  
45  
46  
47  
48  
49  
50  
51  
52  
53  
54  
55  
56  
57  
58  
59  
60

Table 1: Fitting database for the MEAM and MEAM-BO parameters.

Target properties	Data type	Source	Calculation method	Related MEAM parameters
<b>• Saturated hydrocarbon</b>				
Elastic constants of diamond	Expt.	Grimsditch and Ramdas <sup>16</sup>	-	C
Carbon phase: HCP	FP	Yin and Cohen <sup>17</sup>	Norm-conserving pseudopotential <sup>61</sup>	C
Carbon phases: linear chain, simple cubic, BCC, FCC	FP	Perriot <i>et al.</i> <sup>18</sup>	Not specified	C
Energy/bond length/bond angle of Alkane group	Expt.	NIST <sup>31</sup>	-	C, H, CH
H-C-H bond angle of CH <sub>3</sub> radical	Expt.	NIST <sup>31</sup>	-	CH
Dissociation energy of H <sub>2</sub>	FP	Current work	CCSD(2) with aug-cc-pVTZ basis <sup>24,25</sup>	H
Dissociation energy of CH <sub>4</sub> (homogenous deformation)	FP	Current work	CCSD(2) with aug-cc-pVTZ basis <sup>24,25</sup>	CH
Potential energy of H <sub>2</sub> dimer	FP	Burton and Senff <sup>20</sup>	CEPA-PNO <sup>26</sup>	H
Potential energy of CH <sub>4</sub> dimer	FP	Szczesniak <i>et al.</i> <sup>21</sup>	IMPPT/MPPT <sup>27,28</sup>	H
Potential energy of C <sub>2</sub> H <sub>6</sub> dimer	FP	Rowley <i>et al.</i> <sup>22</sup>	MP2/6-311+G(2df,2pd) <sup>29,30</sup>	H
Potential energy of C <sub>3</sub> H <sub>8</sub> dimer	FP	Jalkanen <i>et al.</i> <sup>23</sup>	MP2/6-311+G(2df,2pd) <sup>29,30</sup>	H
Rotational energy barrier of C <sub>2</sub> H <sub>6</sub>	FP	Current work	CCSD(2) with aug-cc-pVTZ basis <sup>24,25</sup>	C,H,CH
Rotational energy barrier of C <sub>4</sub> H <sub>10</sub>	Expt.	Herrebout <i>et al.</i> <sup>32</sup>	-	C,H,CH
Pressure of CH <sub>4</sub> dense system of 0.5534 g/cm <sup>3</sup> at 373K	Expt.	Cristancho <i>et al.</i> <sup>38</sup>	-	H
<b>• Unsaturated hydrocarbon</b>				
Dissociation energy of C <sub>2</sub> H <sub>2</sub>	FP	Current work	CCSD(2) with aug-cc-pVTZ basis <sup>24,25</sup>	Triple bond
Dissociation energy of C <sub>2</sub> H <sub>4</sub>	FP	Current work	CCSD(2) with aug-cc-pVTZ basis <sup>24,25</sup>	Double bond
Dissociation energy of benzene	FP	Current work	CCSD(2) with aug-cc-pVTZ basis <sup>24,25</sup>	Double bond
Dissociation energy of graphene	FP	Current work	GGA-PBE/RRKJ pseudopotential <sup>37,59</sup>	Double bond
Elastic constants of graphene	FP	Wei <i>et al.</i> <sup>36</sup>	GGA-PBE functional <sup>37,59</sup>	Double bond
Atomization energy of graphite	Expt.	Brewer <sup>33</sup>	-	vdW
Elastic constants of graphite	Expt.	Kelly <sup>35</sup>	-	vdW
Interplane distance of graphite	Expt.	Zhao and Spain <sup>34</sup>	-	vdW
Bending energy barrier of C <sub>2</sub> H <sub>2</sub>	FP	Current work	CCSD(2) with aug-cc-pVTZ basis <sup>24,25</sup>	Triple bond
Rotational energy barrier of C <sub>2</sub> H <sub>4</sub>	FP	Current work	CCSD(T) with aug-cc-pVTZ basis <sup>24,25</sup>	Double bond
-: irrelevant information				

Table 2: Weight constants with units and target values used in the downhill simplex method for C and CH parameters of the saturated hydrocarbon system. Cohesive energies/bond lengths/bond angles of alkane group are used to reduce the overall discrepancy between the calculation and the experimental data where the energy is adjusted by the ZPE. C-C bond lengths and C-C-C bond angles are weighted more than other bond lengths and bond angles due to their greater importance. The energies of carbon phases relative to the energy of equilibrium diamond cubic are targeted to make sure that the diamond cubic structure is more stable than the other structures. The weights are appropriately adjusted due to the large unit value of GPa.  $B$ ,  $C_{44}$  and  $C'$  of the diamond cubic structure are used to correct the elastic constants of the structure. The H-C-H angles of  $\text{CH}_3$  are bounded to  $120^\circ$  so that the molecule is planar. Similarly, the H-C-H angles of  $\text{CH}_4+\text{H}$  or  $\text{H}_2$  are regularized to be  $109.47^\circ$ , which is the experimental H-C-H angle for  $\text{CH}_4$ . The peak energy of the rotation barriers for  $\text{C}_2\text{H}_6$  and all available data points for  $\text{C}_4\text{H}_{10}$  are weighted with relatively low values because of their smaller importance. Finally, the net force on all atoms is forced to have close to a zero value to avoid a minimization failure due to the wrong parameterization.

Property	Target value	Unit	Weight
Energies of alkane molecules in Table 9	Expt. + ZPE	eV/molecule	10
C-H bond length of alkane molecules in Table 10	Expt.	Å	100
C-C bond length of alkane molecules in Table 10	Expt.	Å	200
H-C-H and H-C-C bond angles of alkane molecule in Table 11	Expt.	degree	0.05
C-C-C bond angles of alkane molecule in Table 11	Expt.	degree	0.07
Relative energies of carbon phases in Table 8	FP	eV/atom	0.1
$B$ of diamond in Table 8	443.0	GPa	0.01
$C_{44}$ of diamond in Table 8	577.4	GPa	0.001
$C'$ of diamond <sup>a</sup> in Table 8	475.6	GPa	0.001
H-C-H bond angles of $\text{CH}_3$ radical in Table 11	120.00	degree	0.1
H-C-H bond angles of $\text{CH}_5$ and $\text{CH}_6$ radical in Figure 3	109.47	degree	0.02
Peak of rotational energy barrier of $\text{C}_2\text{H}_6$ in Figure 10	0.1145	eV/molecule	1
RMS of energies of all available angles of $\text{C}_4\text{H}_{10}$ in Figure 10	Expt.	eV/molecule	1
$\ell_2$ norm of net force of all atoms	0	(eV/Å) <sup>2</sup>	0.001

$$^a C' = (C_{11} - C_{12})/2$$

Table 3: Single element MEAM parameters for carbon and hydrogen with diamond and diatomic H<sub>2</sub> reference structures, respectively.  $E_{\tau}^0$  (eV) is the cohesive energy per atom,  $R_{\tau}^0$  (Å) is the nearest neighbor distance in the equilibrium reference structure,  $\alpha_{\tau}^0$  is the exponential decay factor in the UEOS,  $\rho_{\tau}^0$  is the electron density scaling factor for the embedding function,  $A_{\tau}^0$  is the embedding function scaling factor,  $\delta_{\tau}^a$  and  $\delta_{\tau}^r$  are the attraction and repulsion cubic terms in the UEOS,  $\beta_{\tau}^{(0-3)}$  are the exponential decay factors for the atomic electron densities,  $t_{\tau}^{(1-3)}$  are the weighting parameters for the atomic electron densities, and  $C_{\min}$  and  $C_{\max}$  are the screening parameters for three like atoms of the element  $\tau$ .

Element	$E_{\tau}^0$	$R_{\tau}^0$	$\alpha_{\tau}^0$	$\rho_{\tau}^0$	$A_{\tau}^0$	$\delta_{\tau}^a$	$\delta_{\tau}^r$	$\beta_{\tau}^{(0)}$	$\beta_{\tau}^{(1)}$	$\beta_{\tau}^{(2)}$	$\beta_{\tau}^{(3)}$	$t_{\tau}^{(1)}$	$t_{\tau}^{(2)}$	$t_{\tau}^{(3)}$	$C_{\min}$	$C_{\max}$
C	7.522	1.540	4.332	1	0.970	0.020	0	3.088	2.790	3.277	3.578	0.645	0.827	-2.207	0.830	2.064
H	2.363	0.740	2.039	2.185	2.123	0	0.050	3.114	2.330	3.673	5.174	0.966	0.395	-0.128	0.750	2.800

Table 4: MEAM interaction and screening parameters for carbon-hydrogen with the methane reference structure.  $E_{\text{CH}}^0$  (eV) is the cohesive energy per atom,  $R_{\text{CH}}^0$  (Å) is the C-H bond distance,  $\alpha_{\text{CH}}^0$  is the exponential decay factor in the UEOS,  $\delta_{\text{CH}}^a$  and  $\delta_{\text{CH}}^r$  are the attraction and repulsion cubic terms in the UEOS, respectively, and  $C_{\text{min}}$  and  $C_{\text{max}}$  are the parameters for the screening factor. The middle atom screens the other two atoms.

C-H parameter	Value
$E_{\text{CH}}^0$	3.6464
$R_{\text{CH}}^0$	1.087
$\alpha_{\text{CH}}^0$	2.946
$\delta_{\text{CH}}^a$	0.048
$\delta_{\text{CH}}^r$	0.030
$C_{\text{min}}(\text{C,C,H})$	1.515
$C_{\text{max}}(\text{C,C,H})$	2.800
$C_{\text{min}}(\text{C,H,C})$	2.000
$C_{\text{max}}(\text{C,H,C})$	2.800
$C_{\text{min}}(\text{C,H,H})$	2.010
$C_{\text{max}}(\text{C,H,H})$	2.800
$C_{\text{min}}(\text{H,C,H})$	0.541
$C_{\text{max}}(\text{H,C,H})$	2.039

**Table 5: MEAM bond parameters for the double bond with ethylene, benzene, and graphene reference structures and for the triple bond with acetylene reference structure. The bond order  $BO$  and the experimental C-C bond lengths  $R_{\text{bond}}$  are given. The  $r_l$  are expansion parameters for the determination of the double bond length, and the  $g_{kl}$  are expansion parameters for the double bond energy increments. The  $e_k$  are expansion parameters for the triple bond increments. The  $\beta_{\text{bond}}^{(0,1,3)}$  are the exponential decay factors for the  $D(z)$  function and bond increment function. The  $p_{\text{bond}}^{(0,1,3)}$  are the power in the  $D(z)$  function.**

Bond Type	$BO$	$R_{\text{bond}}$	$\beta_{\text{bond}}^{(0)}$	$\beta_{\text{bond}}^{(1)}$	$\beta_{\text{bond}}^{(2)}$	$\beta_{\text{bond}}^{(3)}$	$p_{\text{bond}}^{(0)}$	$p_{\text{bond}}^{(1)}$	$p_{\text{bond}}^{(3)}$	k/l	$r_l$	$g_{kl} / e_k$		
												0	1	2
	2	1.339								0	1.3396	-1.296	-4.618	-14.210
double	3/2	1.397	5	1	4.50	1.20	1	1	1.2	1	-0.0959	-0.632	-4.462	21.841
	4/3	1.420								2	0.0364	0.299	-5.452	55.653
triple	3	1.203	5	5	4.50	0.46	1	1	1	-	-	-3.647	-3.030	-13.003

Table 6: The van der Waals parameters for C-C interactions used in Eq. (23).  $e_{\text{vdW}}$  is the van der Waals binding energy,  $r_{\text{vdW}}$  is the position of the van der Waals minimum, and  $\hat{r}_{\text{vdW}}$  is the radial cutoff used in calculating the counting factors.

vdW parameters	Value
$e_{\text{vdW}}$	0.438
$r_{\text{vdW}}$	3.008
$\hat{r}_{\text{vdW}}$	3.300

**Table 7: Overview of the parameterization procedure and parameters to be determined for hydrocarbons using the MEAM formalism.**

Parametrization procedure	Parameters to be determined
<ul style="list-style-type: none"> <li>Saturated hydrocarbon           <ol style="list-style-type: none"> <li>Obtain the UEOS parameters for C, H, and CH in Eq. (8) by fitting the bulk modulus, energy, and lattice constant of the diamond cubic structure and the dissociation energy curve of H<sub>2</sub> and CH<sub>4</sub>.</li> <li>Obtain the remaining C parameters using the direct grid search method and the downhill simplex method for the target elastic constants of the diamond cubic structure and the energies of carbon phases.</li> <li>Adjust the C and CH parameters using the downhill simplex method for all target properties, e.g., atomization energies, bond lengths, and bond angles of the alkane group, with the weights specified in Table 2.</li> <li>Adjust the H parameters for the target dimer interaction energy curves.</li> <li>Iterate Steps 1 through 4 for further improvement.</li> <li>Adjust <math>\beta_{\text{H}}^{(1)}</math> for the pressures of the dense systems</li> </ol> </li> <li>Unsaturated hydrocarbon           <ol style="list-style-type: none"> <li>Fit the bond energy increment<sup>a</sup> in Eq. (32) for C<sub>2</sub>H<sub>2</sub>, C<sub>2</sub>H<sub>4</sub>, benzene, and graphene by Eq. (22) using the experimental bond lengths as an initial guess</li> <li>Fit the experimental double bond lengths as a function of bond order to obtain <math>r_l</math> in Eq. (24)</li> <li>Fit the bond order dependence for double bond to obtain <math>g_{kl}</math> parameters in Eq. (25) based on the three <math>e_k</math> for C<sub>2</sub>H<sub>4</sub>, benzene, and graphene</li> <li>Adjust <math>\beta_{\text{bond}}^{(2)}</math> parameters for double/triple bond to make smooth transition from unsaturated energy to saturated energy in Eq. (22) and Eq. (23)</li> <li>Adjust <math>\beta_2^{(1)}</math>, <math>\beta_2^{(2)}</math> double bond parameters to correct the elastic constants for graphene</li> <li>Iterate Step 7 through 11 for further improvement</li> <li>Adjust the van der Waals parameters in Eq. (28) to correct the equilibrium A-B stack distance of graphite and its energy curvature.</li> <li>Adjust <math>\beta_{\text{bond}}^{(3)}</math> and <math>p_{\text{bond}}^{(3)}</math> parameters of the <math>D(z)</math> functions in Eq. (21) to correct the shape of C<sub>2</sub>H<sub>4</sub> rotation barrier energy curve and C<sub>2</sub>H<sub>2</sub> bending barrier energy curve.</li> </ol> </li> </ul>	$R_{\text{C/H/CH}}^0, E_{\text{C/H/CH}}^0, \alpha_{\text{C/H/CH}}^0, \delta_{\text{C/H/CH}}^a, \delta_{\text{C/H/CH}}^r$ $A_{\text{C}}^0, \beta_{\text{C}}^{(0-3)}, t_{\text{C}}^{(1-3)}, C_{\text{min}}(\text{C}, \text{C}, \text{C}), C_{\text{max}}(\text{C}, \text{C}, \text{C})$ $A_{\text{C}}^0, \beta_{\text{C}}^{(0-3)}, t_{\text{C}}^{(1-3)}, \rho_{\text{H}}^0, C_{\text{min}}(\text{C}, \text{C}, \text{H}), C_{\text{min}}(\text{C}, \text{H}, \text{H}), C_{\text{min}}(\text{H}, \text{C}, \text{H}), C_{\text{max}}(\text{C}, \text{H}, \text{H}), C_{\text{min}}(\text{H}, \text{C}, \text{H})$ $A_{\text{H}}^0, \beta_{\text{H}}^{(0-3)}, t_{\text{H}}^{(1-3)}, \delta_{\text{H}}^a$ $\beta_{\text{H}}^{(1)}$ $e_0, e_1, e_2$ for four reference structures $r_1, r_2, r_3$ $g_{00}, g_{01}, g_{02}, g_{10}, g_{11}, g_{12}, g_{20}, g_{21}, g_{22}$ $\beta_2^{(2)}, \beta_3^{(2)}$ $\beta_2^{(1)}, \beta_2^{(2)}$ $r_{\text{vdW}}, e_{\text{vdW}}$ $\beta_2^{(3)}, p_2^{(3)}, \beta_3^{(3)}, p_3^{(3)}$

<sup>a</sup> the van der Waals term for graphite is set to zero at Step 7, which is obtained in Step 14

**Table 8: Carbon properties calculated from MEAM (previous work<sup>9</sup> and current work) and experimental data. Current work includes unsaturated bond energies and are denoted as MEAM-BO. The zero-point energy (ZPE) corrections used here are 0.166 eV/atom for graphene and graphite<sup>62,63</sup> and of 0.176 eV/atom for diamond<sup>64</sup> for the MEAM and REBO potentials while the empirical heat increment value, 1.254eV/atom, is used for diamond, graphene, and graphite as the energy correction for ReaxFF.  $E_{\text{Corr}}$  is the corrected energy either by ZPE or empirical heat increment value (experimental energy is not corrected).  $\Delta E_{\text{star} \rightarrow \text{DC}}$  is the equilibrium cohesive energy relative to the cohesive energy of the diamond structure. Additional structures examined are the linear chain (LC), simple cubic (SC), body-centered cubic (BCC), hexagonal close-packed (HCP), and face-centered cubic (FCC).**

Species	Property	Expt.	MEAM-BO		MEAM(prev.)		REBO		ReaxFF	
			Calc.	Diff.	Calc.	Diff.	Calc.	Diff.	Calc.	Diff.
Diamond	$E_{\text{Corr}}$ (eV/atom)	7.346 <sup>a</sup>	7.346	0	7.194	-0.152	7.280	-0.066	7.375	0.030
	Lattice const.(Å)	3.567	3.567	0	3.325	-0.242	3.558	-0.009	3.619	0.052
	Atomic volume(Å <sup>3</sup> )	5.673	5.673	0	4.595	-1.078	5.628	-0.045	5.924	0.251
	$B$ (GPa)	443.0	442.2	-0.8	369.1	-73.9	452.1	9.1	40970	40527
	$C_{11}$ (GPa)	1076.4 <sup>b</sup>	815.9	-260.5	405.3	-671.1	1114.7	38.3	41306	40230
	$C_{12}$ (GPa)	125.2 <sup>b</sup>	255.4	130.2	351.0	225.8	120.8	-4.4	40802	40677
	$C_{44}$ (GPa)	577.4 <sup>b</sup>	489.5	-87.9	63.5	-513.9	754.5	177.1	438.5	-138.9
	$C'$ (GPa)	475.6 <sup>c</sup>	280.2	-195.4	27.2	-448.4	497.0	21.3	252.0	-223.6
	<b>RMS error</b>	-	-	<b>127.8</b>	-	<b>348.5</b>	-	<b>64.6</b>	-	<b>24788.3</b>
<b>MAP<sup>l</sup> error</b>	-	-	<b>23.1</b>	-	<b>58.8</b>	-	<b>5.8</b>	-	<b>5681.7</b>	
LC	$\Delta E_{\text{LC} \rightarrow \text{DC}}$ (eV/atom)	0.823 <sup>d</sup>	3.125	2.302	2.912	2.089	1.338	0.515	1.392	0.569
SC	$\Delta E_{\text{SC} \rightarrow \text{DC}}$ (eV/atom)	2.637 <sup>d</sup>	1.345	-1.292	-1.134	-3.771	4.651	2.014	2.889	0.252
BCC	$\Delta E_{\text{BCC} \rightarrow \text{DC}}$ (eV/atom)	4.331 <sup>d</sup>	3.217	-1.114	-2.759	-7.090	4.579	0.248	4.612	0.281
HCP	$\Delta E_{\text{HCP} \rightarrow \text{DC}}$ (eV/atom)	4.48 <sup>e</sup>	2.599	-1.881	-5.680	-10.160	4.786	0.306	3.394	-1.086
FCC	$\Delta E_{\text{FCC} \rightarrow \text{DC}}$ (eV/atom)	4.486 <sup>d</sup>	2.622	-1.864	-5.657	-10.143	4.695	0.209	3.448	-1.038
	<b>RMS error</b>	-	-	<b>1.745</b>	-	<b>7.416</b>	-	<b>0.951</b>	-	<b>0.738</b>
	<b>MAP<sup>l</sup> error</b>	-	-	<b>87.6</b>	-	<b>202.7</b>	-	<b>31.2</b>	-	<b>26.5</b>
Graphene	$E_{\text{Corr}}$ (eV/atom)	7.315 <sup>f</sup>	7.304	-0.011	5.761	-1.554	7.243	-0.072	6.884	0.431
	Lattice const., a (Å)	2.462 <sup>g</sup>	2.46	-0.002	2.413	-0.049	2.419	-0.043	2.501	0.041
	$C_{11} + C_{12}$ (N/m)	358.1 <sup>h</sup>	363.4	5.3	228.7	-129.4	436.9	78.8	744787	744428
	$C_{66}$ (N/m)	60.4 <sup>h</sup>	134.9	74.5	21.1	-39.3	194.0	133.6	193449	193388
	Young's modulus (GPa)	1020 <sup>i</sup>	923 <sup>k</sup>	-97	213 <sup>k</sup>	-781	1141 <sup>k</sup>	121	47837 <sup>k</sup>	46817
	Poisson's ratio	0.165 <sup>i</sup>	0.151	-0.014	0.689	0.524	0.126	-0.039	0.979	0.814
	<b>RMS error</b>	-	-	<b>50.1</b>	-	<b>334.1</b>	-	<b>80.3</b>	-	<b>314580</b>
	<b>MAP<sup>l</sup> error</b>	-	-	<b>23.8</b>	-	<b>86.9</b>	-	<b>46.9</b>	-	<b>88858</b>
	Graphite	$E_{\text{Corr}}$ (eV/atom)	7.371 <sup>a</sup>	7.372	0.001	7.489	0.118	7.311	-0.060	7.413
Lattice const., a (Å)		2.462 <sup>g</sup>	2.47	0.008	2.753	0.293	2.418	-0.042	2.501	0.041
Lattice const., c (Å)		6.707 <sup>g</sup>	6.71	0.003	2.910	-3.795	6.713	0.008	6.319	-0.386
$C_{11} + C_{12}$ (GPa)		1240 <sup>j</sup>	1052	-188	-	-	1309	69	2434604	2433364
$C_{66}$ (GPa)		440 <sup>j</sup>	406	-34	-	-	508	69	12822	12382
$C_{13}$ (GPa)		15 <sup>j</sup>	28	13	-	-	0.3	-14.7	7.8	-7.2
$C_{33}$ (GPa)		36.5 <sup>j</sup>	37.1	0.6	-	-	41.0	4.5	1082.5	1046.0
$C_{44}$ (GPa)		4.5 <sup>j</sup>	293.6	289.1	-	-	0.1	-4.4	4.9	0.4
<b>RMS error</b>		-	-	<b>122.6</b>	-	-	-	<b>34.7</b>	-	<b>860335</b>
<b>MAP<sup>l</sup> error</b>		-	-	<b>817.0</b>	-	-	-	<b>29.0</b>	-	<b>25247</b>
<b>MAP<sup>l</sup> error (except <math>C_{44}</math>)</b>	-	-	<b>15.9</b>	-	-	-	<b>19.1</b>	-	<b>28854</b>	

<sup>a</sup> Brewer<sup>33</sup>, <sup>b</sup> Grimsditch and Ramdas<sup>16</sup>, <sup>c</sup>  $C' = (C_{11} - C_{12})/2$ , <sup>d</sup> Perriot *et al.* (calc.)<sup>18</sup>, <sup>e</sup> Yin and Cohen (calc.)<sup>17</sup>, <sup>f</sup> Shin *et al.* (calc.)<sup>65</sup>, <sup>g</sup> Zhao and Spain<sup>34</sup>, <sup>h</sup> Wei *et al.* (calc.)<sup>36</sup>, <sup>i</sup> Lee *et al.*<sup>51</sup>, <sup>j</sup> Kelly<sup>35</sup>, <sup>k</sup> Stacking distance of graphite 3.35 Å is divided to compare with the experimental data, <sup>l</sup> Mean absolute percentage error given in Eq. (34)

**Table 9: Atomization energies of various isomer groups at 0K from MEAM, REBO, and ReaxFF calculations and experimental data. Adjustments were made for each potential by ZPE (MEAM, REBO) or empirical heat increment (ReaxFF)**

Group	Molecule	Expt. <sup>a</sup> (eV)	ZPE <sup>b</sup> (eV)	Heat inc. <sup>c</sup> (eV)	MEAM-BO		REBO		ReaxFF		
					Calc. (eV)	Corr. (eV)	Calc. (eV)	Corr. (eV)	Calc. (eV)	Corr. (eV)	
Alkane	Methane	<b>17.018</b>	1.214	2.592	18.232	<b>17.018</b>	18.185	<b>16.971</b>	20.092	<b>17.499</b>	
	Ethane	<b>28.885</b>	2.023	4.515	30.941	<b>28.918</b>	30.846	<b>28.823</b>	34.453	<b>29.937</b>	
	Propane	<b>40.880</b>	2.803	6.439	43.723	<b>40.92</b>	43.593	<b>40.790</b>	48.732	<b>42.294</b>	
	<i>n</i> -Butane	<b>52.896</b>	3.578	8.362	56.503	<b>52.925</b>	56.347	<b>52.769</b>	63.020	<b>54.658</b>	
	Isobutane	<b>52.977</b>	3.564	8.362	56.559	<b>52.995</b>	56.340	<b>52.776</b>	63.030	<b>54.669</b>	
	<i>n</i> -Pentane	<b>64.915</b>	4.351	10.285	69.282	<b>64.931</b>	69.102	<b>64.751</b>	77.308	<b>67.023</b>	
	Isopentane	<b>64.964</b>	4.338	10.285	69.328	<b>64.99</b>	69.050	<b>64.712</b>	77.325	<b>67.040</b>	
	Neopentane	<b>65.123</b>	4.319	10.285	69.416	<b>65.097</b>	69.074	<b>64.755</b>	77.711	<b>67.426</b>	
	<i>n</i> -Hexane	<b>76.922</b>	5.123	12.208	82.062	<b>76.939</b>	81.858	<b>76.735</b>	91.593	<b>79.385</b>	
	Isohexane	<b>76.975</b>	5.113	12.208	82.072	<b>76.959</b>	81.677	<b>76.564</b>	91.541	<b>79.333</b>	
	3-Methylpentane	<b>76.946</b>	5.114	12.208	82.071	<b>76.957</b>	81.742	<b>76.628</b>	91.540	<b>79.332</b>	
	2,3-Dimethylbutane	<b>76.970</b>	5.101	12.208	82.119	<b>77.018</b>	81.701	<b>76.600</b>	91.532	<b>79.324</b>	
	Neohexane	<b>77.060</b>	5.098	12.208	82.145	<b>77.047</b>	81.723	<b>76.625</b>	91.955	<b>79.748</b>	
	<i>n</i> -Heptane	<b>88.957</b>	5.896	14.131	94.841	<b>88.945</b>	94.614	<b>88.718</b>	105.886	<b>91.755</b>	
	Isoheptane	<b>89.008</b>	5.881	14.131	94.81	<b>88.929</b>	94.370	<b>88.489</b>	105.874	<b>91.743</b>	
	<i>n</i> -Octane	<b>100.971</b>	6.668	16.054	107.62	<b>100.952</b>	107.369	<b>100.701</b>	120.174	<b>104.120</b>	
		<b>RMS error</b>	-	-	-	-	<b>0.031</b>	-	<b>0.288</b>	-	<b>2.217</b>
	<b>MAP error</b>	-	-	-	-	<b>0.1</b>	-	<b>0.4</b>	-	<b>3.2</b>	
Cycloalkane	Cyclopropane	<b>34.818</b>	2.207	5.769	37.26	<b>35.053</b>	36.772	<b>34.565</b>	41.596	<b>35.827</b>	
	Cyclobutane	<b>46.848</b>	3.005	7.692	50.566	<b>47.561</b>	49.233	<b>46.228</b>	56.272	<b>48.579</b>	
	Cyclopentane	<b>59.707</b>	3.814	9.615	63.758	<b>59.944</b>	62.850	<b>59.036</b>	71.095	<b>61.479</b>	
	Cyclohexane	<b>71.963</b>	4.617	11.538	76.672	<b>72.055</b>	76.457	<b>71.840</b>	85.732	<b>74.193</b>	
		<b>RMS error</b>	-	-	-	-	<b>0.397</b>	-	<b>0.478</b>	-	<b>1.742</b>
		<b>MAP error</b>	-	-	-	-	<b>0.7</b>	-	<b>0.8</b>	-	<b>3.2</b>
Alkene	Ethene (ethylene)	<b>23.066</b>	1.385	3.846	23.445	<b>23.070</b>	24.420	<b>23.035</b>	27.829	<b>23.982</b>	
Alkyne	Ethyne (acetylene)	<b>16.857</b>	0.735	3.177	17.591	<b>16.856</b>	17.565	<b>16.830</b>	20.600	<b>17.423</b>	
Aromatic	Benzene	<b>56.619</b>	2.732	9.531	59.369	<b>56.637</b>	59.075	<b>56.343</b>	67.236	<b>57.705</b>	
Radical	CH	<b>3.469</b>	0.175	1.588	6.659	<b>6.484</b>	4.526	<b>4.351</b>	5.148	<b>3.559</b>	
	CH <sub>2</sub>	<b>7.410</b>	0.467	1.923	10.654	<b>10.187</b>	8.469	<b>8.002</b>	10.148	<b>8.225</b>	
	CH <sub>3</sub>	<b>12.534</b>	0.807	2.258	14.52	<b>13.694</b>	13.375	<b>12.549</b>	15.279	<b>13.021</b>	
	C <sub>2</sub> H	<b>11.125</b>	0.383	2.842	12.335	<b>11.952</b>	11.572	<b>11.189</b>	14.351	<b>11.509</b>	
	H <sub>3</sub> C <sub>2</sub> H <sub>2</sub>	<b>24.572</b>	1.612	4.181	27.345	<b>25.733</b>	26.550	<b>24.938</b>	29.805	<b>25.625</b>	
	CH <sub>3</sub> CHCH <sub>3</sub>	<b>36.676</b>	2.382	6.104	40.228	<b>37.846</b>	39.481	<b>37.099</b>	44.030	<b>37.926</b>	
		<b>RMS error</b>	-	-	-	-	<b>1.896</b>	-	<b>0.491</b>	-	<b>0.789</b>
	<b>MAP error</b>	-	-	-	-	<b>24.8</b>	-	<b>6.1</b>	-	<b>4.8</b>	

<sup>a</sup> From the NIST Computational Chemistry Comparison and Benchmark Database<sup>31</sup><sup>b</sup> Authors (calc.) B3LYP/cc-pVTZ<sup>c</sup>  $E_{inc,CH} = (E_{expt,C} - E_{inc,C}) \cdot N_C + (E_{expt,H} - E_{inc,H}) \cdot N_H$ , where  $E_{inc,CH}$  is heat increment energy for hydrocarbon,  $E_{expt,C}$  and  $E_{expt,H}$  are the experimental energies for carbon (7.3768 eV) and hydrogen (2.375 eV),<sup>45</sup>  $E_{inc,C}$  and  $E_{inc,H}$  are the empirical heat increments for carbon (8.6306 eV) and hydrogen (2.7097 eV),<sup>48</sup> and  $N_C$  and  $N_H$  are the number of atoms for carbon and hydrogen.

**Table 10: Average equilibrium C–H and C–C bond length for select molecules after energy minimization using the MEAM, REBO, and ReaxFF potentials. The results are compared to experimental data.**

Group	Molecule	C-H bond length(Å)				C-C bond length(Å)			
		Expt. <sup>a</sup>	MEAM-BO	REBO	ReaxFF	Expt. <sup>a</sup>	MEAM-BO	REBO	ReaxFF
Alkane	Methane	1.087	1.087	1.089	1.099	-	-	-	-
	Ethane	1.094	1.114	1.090	1.096	1.535	1.533	1.543	1.573
	Propane	1.107	1.120	1.090	1.094	1.532	1.537	1.543	1.575
	<i>n</i> -Butane	1.117	1.123	1.090	1.093	1.531	1.538	1.543	1.575
	Isobutane	1.113	1.119	1.090	1.104	1.535	1.541	1.545	1.528
	<i>n</i> -Pentane	1.118	1.125	1.090	1.093	1.531	1.539	1.543	1.575
	Neopentane	1.114	1.113	1.090	1.104	1.537	1.548	1.547	1.530
	<i>n</i> -Hexane	1.118	1.127	1.090	1.093	1.533	1.540	1.544	1.574
	<i>n</i> -Heptane	1.121	1.128	1.090	1.092	1.534	1.540	1.544	1.575
	<b>RMS error</b>	-	<b>0.010</b>	<b>0.023</b>	<b>0.019</b>	-	<b>0.007</b>	<b>0.011</b>	<b>0.036</b>
<b>MAP error</b>	-	<b>0.7</b>	<b>1.8</b>	<b>1.5</b>	-	<b>0.4</b>	<b>0.7</b>	<b>2.2</b>	
Cycloalkane	Cyclopropane	1.083	1.129	1.080	1.089	1.501	1.612	1.656	1.539
	Cyclobutane	1.093	1.135	1.084	1.089	1.555	1.566	1.630	1.578
	Cyclopentane	1.114	1.137	1.088	1.090	1.546	1.542	1.558	1.574
	Cyclohexane	N/A	-	-	-	1.530	1.539	1.543	1.573
	<b>RMS error</b>	-	<b>0.038</b>	<b>0.016</b>	<b>0.015</b>	-	<b>0.056</b>	<b>0.087</b>	<b>0.034</b>
<b>MAP error</b>	-	<b>3.4</b>	<b>1.2</b>	<b>1.1</b>	-	<b>2.2</b>	<b>4.1</b>	<b>2.2</b>	
Alkene	Ethene (ethylene)	1.086	1.110	1.090	1.083	1.339	1.337	1.310	1.334
Alkyne	Ethyne (acetylene)	1.063	1.111	1.090	1.081	1.203	1.202	1.206	1.188
Aromatic	Benzene	1.084	1.140	1.090	1.097	1.397	1.396	1.374	1.418
Radical	CH	1.120	0.967	1.090	1.074	-	-	-	-
	CH <sub>2</sub>	1.085	1.010	1.105	1.078	-	-	-	-
	C <sub>2</sub> H	1.047	1.064	1.090	1.077	1.217	1.442	1.276	1.250
	<b>RMS error</b>	-	<b>0.099</b>	<b>0.032</b>	<b>0.032</b>	-	<b>0.225</b>	<b>0.059</b>	<b>0.033</b>
<b>MAP error</b>	-	<b>7.4</b>	<b>2.9</b>	<b>2.5</b>	-	<b>18.5</b>	<b>4.8</b>	<b>2.8</b>	

<sup>a</sup> From the NIST computational Chemistry Comparison and Benchmark Database<sup>31</sup>

**Table 11: Average equilibrium  $\angle\text{H-C-H}$ ,  $\angle\text{H-C-C}$ , and  $\angle\text{C-C-C}$  bond angles for select molecules after energy minimization using the MEAM, REBO, and ReaxFF potentials. The results are compared to experimental data**

Group	Molecule	$\angle\text{H-C-H}$ bond angle ( $^\circ$ )				$\angle\text{H-C-C}$ bond angle ( $^\circ$ )				$\angle\text{C-C-C}$ bond angle ( $^\circ$ )			
		Expt. <sup>a</sup>	MEAM-BO	REBO	ReaxFF	Expt. <sup>a</sup>	MEAM-BO	REBO	ReaxFF	Expt. <sup>a</sup>	MEAM-BO	REBO	ReaxFF
Alkane	Methane	109.47	109.47	109.47	109.47	-	-	-	-	-	-	-	-
	Ethane	107.70	107.69	108.54	107.19	111.17	111.20	110.39	111.66	-	-	-	-
	Propane	107.00	107.25	108.33	106.98	N/A	-	-	-	111.70	112.18	111.33	106.87
	<i>n</i> -Butane	N/A	-	-	-	111.00	110.30	109.89	111.34	113.80	112.33	111.23	106.90
	Isobutane	N/A	-	-	-	111.40	111.64	110.00	111.82	110.80	111.89	110.34	109.83
	<i>n</i> -Pentane	N/A	-	-	-	110.40	110.07	109.80	111.29	112.90	112.42	111.19	106.91
	Neopentane	106.60	107.15	108.40	107.16	112.20	111.70	110.53	111.70	N/A	-	-	-
	<i>n</i> -Hexane	N/A	-	-	-	109.50	109.92	109.74	111.22	111.90	112.48	111.16	107.18
	<i>n</i> -Heptane	N/A	-	-	-	109.80	109.81	109.70	111.24	112.60	112.52	111.15	106.86
	<b>RMS error</b>	-	<b>0.30</b>	<b>1.19</b>	<b>0.38</b>	-	<b>0.39</b>	<b>1.00</b>	<b>0.97</b>	-	<b>0.83</b>	<b>1.45</b>	<b>5.21</b>
<b>MAP error</b>	-	<b>0.2</b>	<b>0.9</b>	<b>0.3</b>	-	<b>0.3</b>	<b>0.8</b>	<b>0.8</b>	-	<b>0.6</b>	<b>1.1</b>	<b>4.3</b>	
Cycloalkane	Cyclopropane	114.50	107.31	114.83	113.68	117.90	120.88	117.80	118.28	60.00	60.00	60.00	60.00
	Cyclohexane	106.65	106.95	107.23	105.79	N/A	-	-	-	111.28	111.12	110.40	107.19
	<b>RMS error</b>	-	<b>5.09</b>	<b>0.47</b>	<b>0.84</b>	-	<b>2.98</b>	<b>0.10</b>	<b>0.38</b>	-	<b>0.11</b>	<b>0.62</b>	<b>2.89</b>
	<b>MAP error</b>	-	<b>3.3</b>	<b>0.4</b>	<b>0.8</b>	-	<b>2.5</b>	<b>0.1</b>	<b>0.3</b>	-	<b>0.1</b>	<b>0.4</b>	<b>1.8</b>
Alkene	Ethene (ethylene)	117.60	118.27	110.91	116.10	121.20	120.87	124.55	122.00	-	-	-	-
Alkyne	Ethyne (acetylene)	-	-	-	-	180.00	180.00	180.00	180.00	-	-	-	-
Aromatic	Benzene	-	-	-	-	120.00	120.00	120.00	120.00	120.00	120.00	120.00	120.00
Radical	CH <sub>3</sub>	120.00	120.00	120.0	119.39	-	-	-	-	-	-	-	-
	C <sub>2</sub> H	-	-	-	-	180.00	179.12	180.00	180.00	-	-	-	-

<sup>a</sup>From the NIST computational Chemistry Comparison and Benchmark Database<sup>31</sup>

**Table 12: Molecular dynamics results of 3D periodic methane, ethane, propane, and butane systems under the NVT ensemble for a total time of 400 ps simulation. The averages of the last 100 ps results of each system are compared to the experimental data.**

System	No. of atoms	Cell		Temp. (K)	Expt. Pressure (MPa)	MEAM		REBO		ReaxFF	
		length (Å)	Density (g/cm <sup>3</sup> )			Pressure (MPa)	Diff. (MPa)	Pressure (MPa)	Diff. (MPa)	Pressure (MPa)	Diff. (MPa)
Methane-1	5000	102.69	0.0246	400	<b>5.005<sup>a</sup></b>	<b>4.7</b>	-0.3	<b>8.5</b>	3.5	<b>-9.9</b>	-14.9
Methane-2	5000	92.01	0.0342	305	<b>5.00<sup>a</sup></b>	<b>4.4</b>	-0.6	<b>9.3</b>	4.3	<b>-20.9</b>	-25.9
Methane-3	5000	60.80	0.1185	298	<b>14.994<sup>a</sup></b>	<b>10.6</b>	-4.4	<b>30.9</b>	15.9	<b>-74.3</b>	-89.3
Methane-4	5000	50.89	0.2021	450	<b>59.975<sup>a</sup></b>	<b>49.4</b>	-10.5	<b>81.3</b>	21.3	<b>-24.1</b>	-84.0
Methane-5	5000	41.30	0.3782	338	<b>179.829<sup>a</sup></b>	<b>118.1</b>	-61.8	<b>267.2</b>	87.4	<b>33.9</b>	-145.9
Methane-6	5000	40.51	0.4008	298	<b>188.059<sup>a</sup></b>	<b>101.1</b>	-87	<b>299.0</b>	110.9	<b>-1.6</b>	-189.7
Methane-7	5000	36.38	0.5534	373	<b>1000.000<sup>b</sup></b>	<b>959.1</b>	-40.9	<b>1562.9</b>	562.9	<b>727.2</b>	-272.8
Ethane-1	8000	110.41	0.0371	308	<b>2.550<sup>c</sup></b>	<b>2.2</b>	-0.4	<b>5.1</b>	2.5	<b>25.4</b>	22.8
Ethane-2	8000	56.79	0.2726	308	<b>5.387<sup>c</sup></b>	<b>7.4</b>	2.1	<b>29.3</b>	23.9	<b>238.0</b>	232.6
Ethane-3	8000	46.71	0.4901	260	<b>31.294<sup>c</sup></b>	<b>27.3</b>	-4	<b>144.4</b>	113.1	<b>441.3</b>	410.0
Propane	11000	66.44	0.2497	325	<b>26.891<sup>d</sup></b>	<b>4.5</b>	-22.4	<b>10.1</b>	-16.8	<b>31.9</b>	5.0
n-Butane	14000	54.92	0.5827	300	<b>7.089<sup>e</sup></b>	<b>36.3</b>	29.2	<b>115.2</b>	108.1	<b>190.3</b>	183.2
<b>RMS error</b>										<b>34.8</b>	<b>173.9</b>
<b>MAP error</b>										<b>59.2</b>	<b>246.2</b>

<sup>a</sup> Cristancho *et al.*<sup>38</sup>

<sup>b</sup> Robertson and Babb<sup>66</sup>

<sup>c</sup> Straty and Tsumura<sup>67</sup>

<sup>d</sup> Straty and Palavra<sup>68</sup>

<sup>e</sup> Kayukawa *et al.*<sup>69</sup>

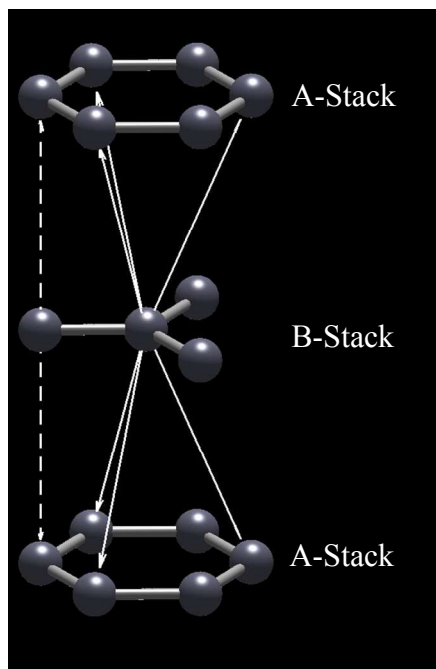


**Figure 1: Two different types of C atoms in graphite. The atom in the B-stack and the two atoms in the A-stacks connected by the dashed line are aligned. The atom at the center of the B-stack and the six atoms in the A-stacks connected by the solid lines are not aligned.**

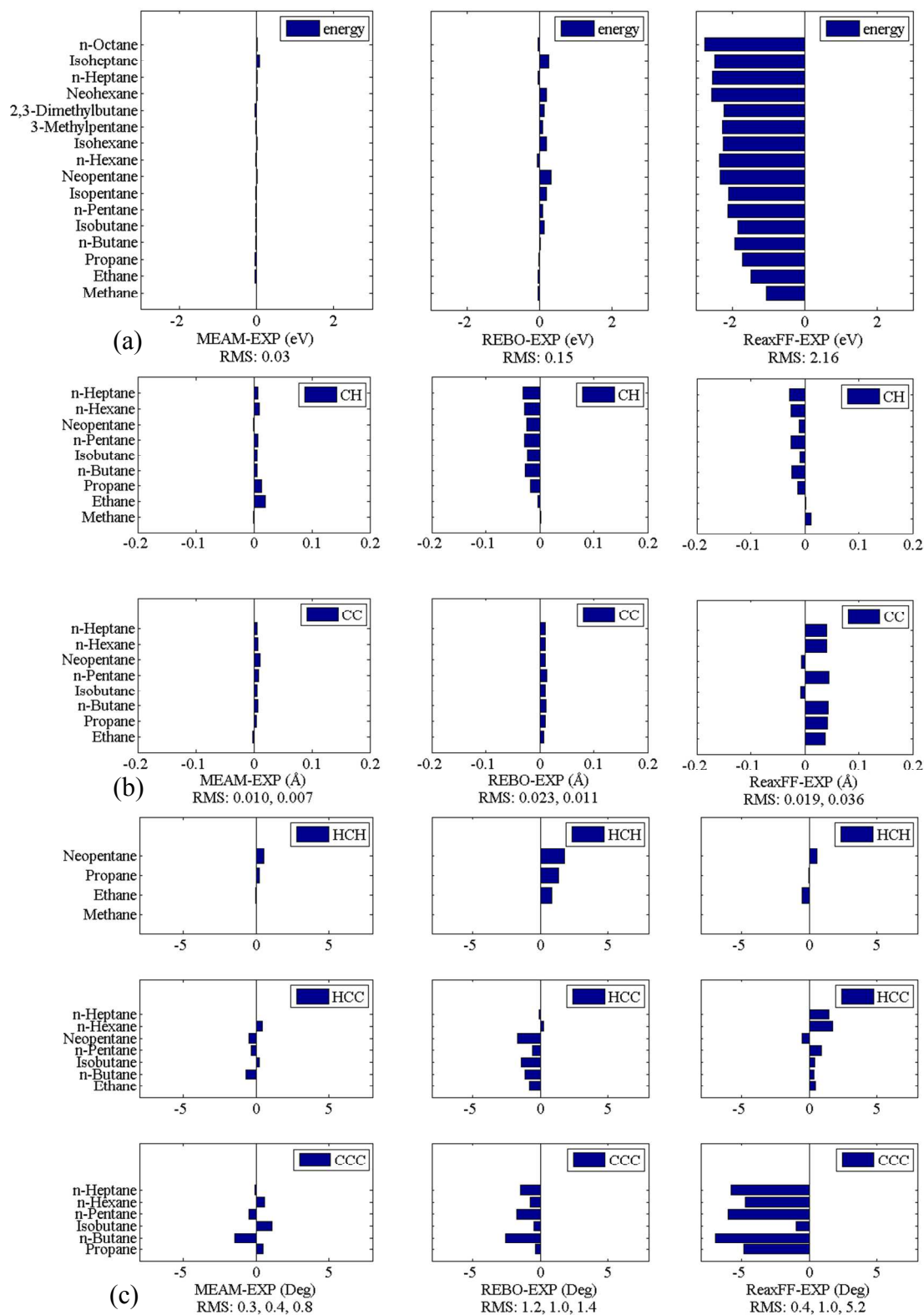
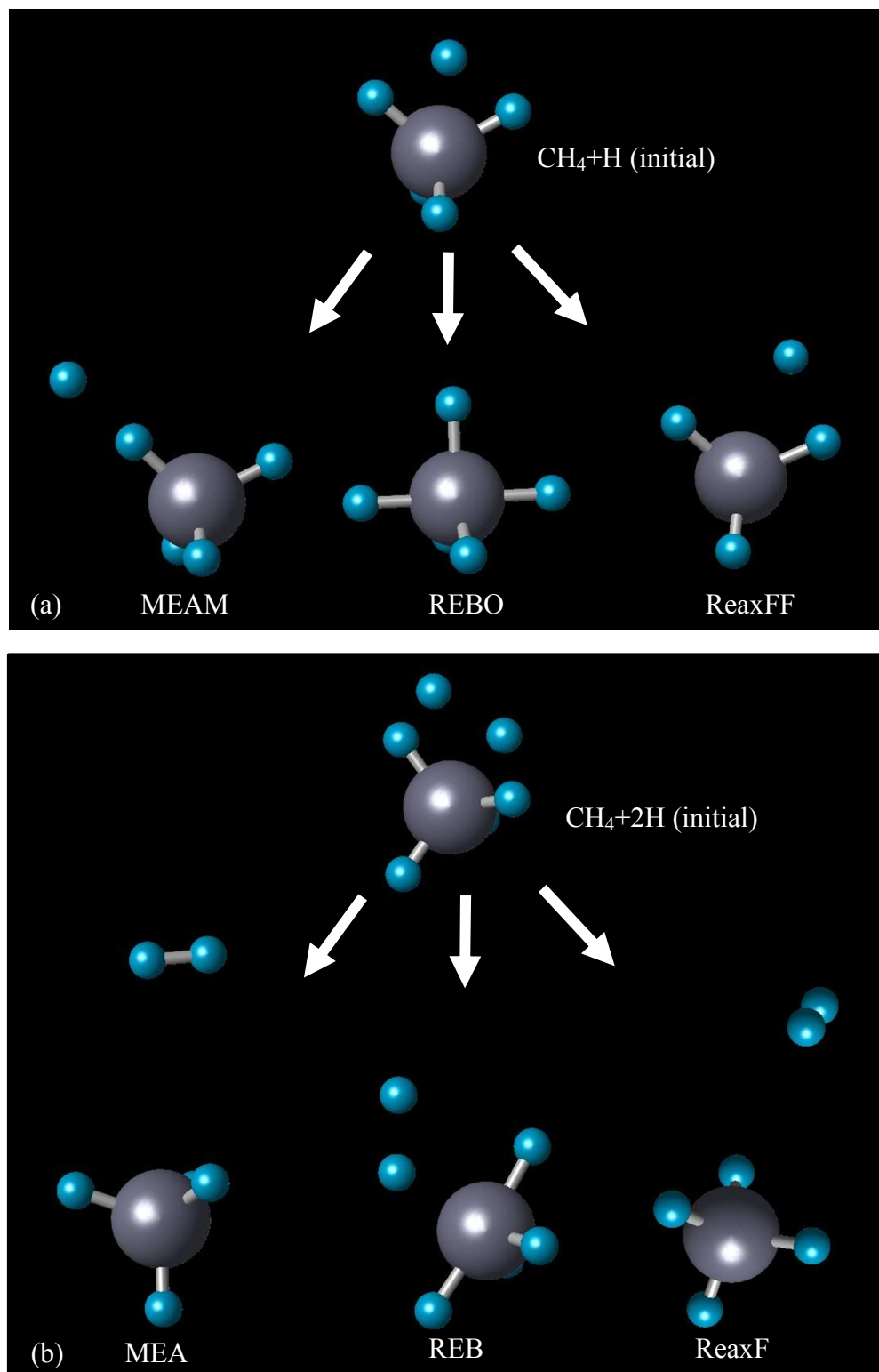


**Figure 2: Differences between the (a) atomization energy's, (b) bond length's, and (c) bond angle's experimental data and MEAM's (first column), REBO's (second column), and ReaxFF's (third column) calculation results. Root Mean Square (RMS) values are given at the bottom of each subfigure. The detailed results are given in Table 9, 10, and 11.**



51  
52  
53  
54  
55  
56  
57  
58  
59  
60

**Figure 3: Results of the “oversaturation” test for (a)  $\text{CH}_4+\text{H}$  and (b)  $\text{CH}_4+2\text{H}$  atomic configurations. The pictures at the top of each subfigure are the initial configurations, and the pictures on the bottom are the resultant structures after energy minimization. The energy minimized structures using the MEAM, REBO, and ReaxFF potentials are presented. The MEAM and ReaxFF results show the successful ejection of hydrogen in both (a) and (b).**

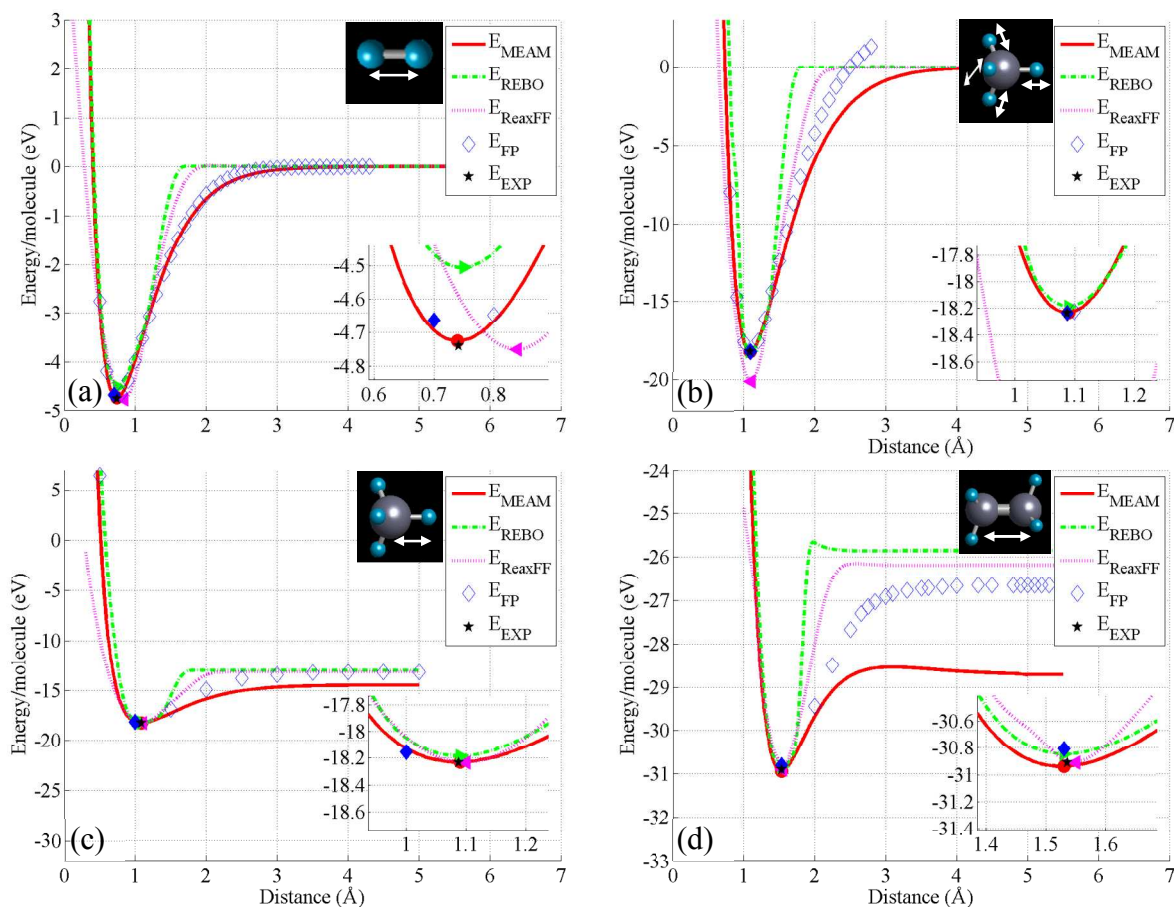


**Figure 4: Potential energy curves of (a) hydrogen, (b) methane (homogenous deformation), (c) methane (disassociation of one H), and (d) ethane. The MEAM results are compared to those of REBO, ReaxFF, FP data ((a) and (b) CCSD(2)/aug-cc-pVTZ<sup>24,25</sup>, (c) and (d) B3LYP XC functional/the 6-31G\*\* basis set<sup>56,57</sup> from the work of Lorant *et al.*<sup>58</sup>) and experimental results. The experimental energies were adjusted by the Zero Point Energies (ZPEs) and are represented as single black stars. Filled markers indicate the minimum of each energy curve near the equilibrium bond length. The small windows at the bottom right corner represent a magnified view of the energy minimum at the equilibrium bond length. The white double arrows in the pictures of the molecules indicate the coordinate that is being varied. For the three C-H bonds that are not varied in (c) and the C-H bonds in (b) and (d) were held to the equilibrium distance with respect to the respective potential.**

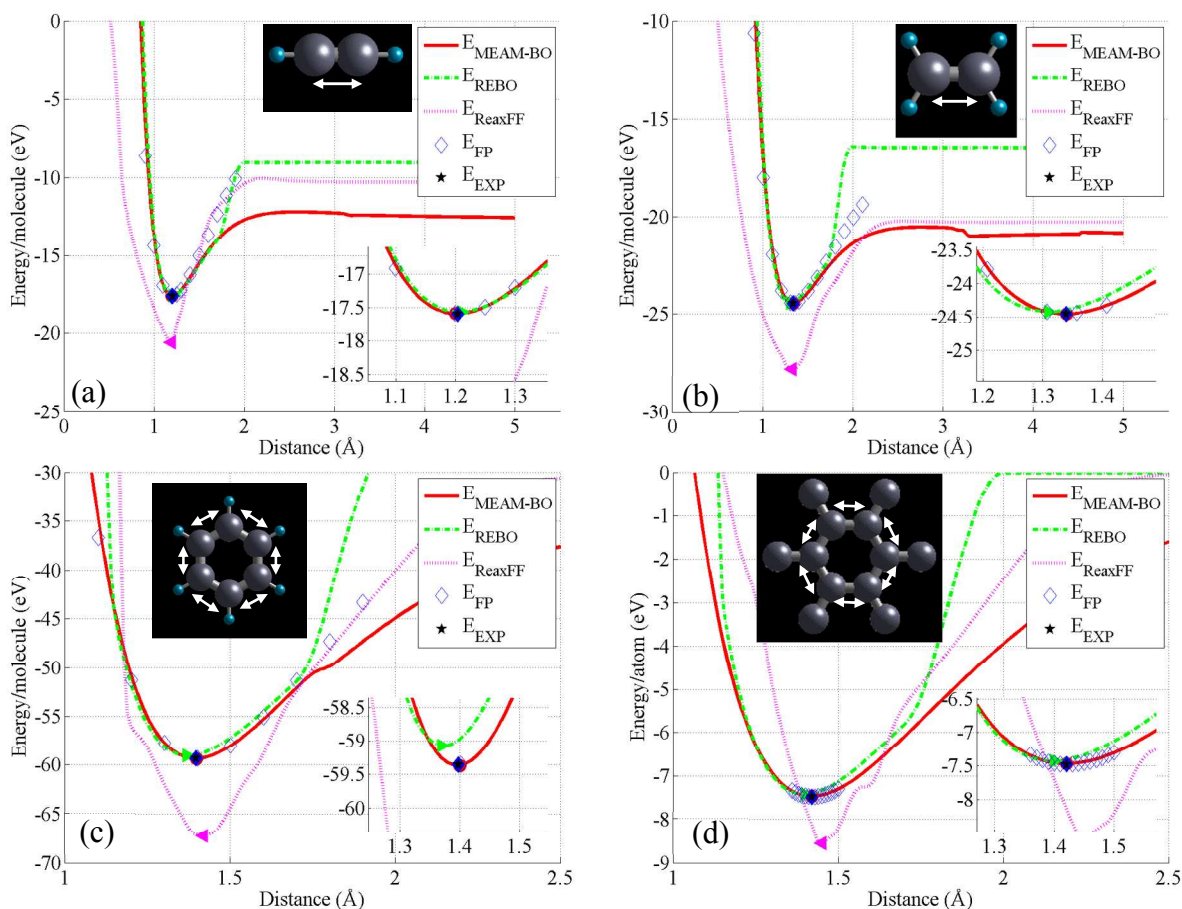


**Figure 5: Potential energy curves of (a) acetylene, (b) ethylene, (c) benzene, and (d) graphene. The MEAM-BO results are compared to those of REBO, ReaxFF, FP data ((a)-(c) CCSD(2)/aug-cc-pVTZ<sup>24,25</sup> (d) PBE XC functional/RRKJ pseudopotential<sup>37,59</sup>) and experimental results. The experimental energies were adjusted by the Zero Point Energies (ZPEs) and are represented as single black stars. Filled markers indicate the minimum of each energy curve near the equilibrium bond length. The small windows at the bottom right corner represent a magnified view of the energy minimum at the equilibrium bond length. The white double arrows in the pictures of the molecules indicate the C-C coordinate that is being varied. The C-H bonds were held to the equilibrium distance with respect to the respective potential.**

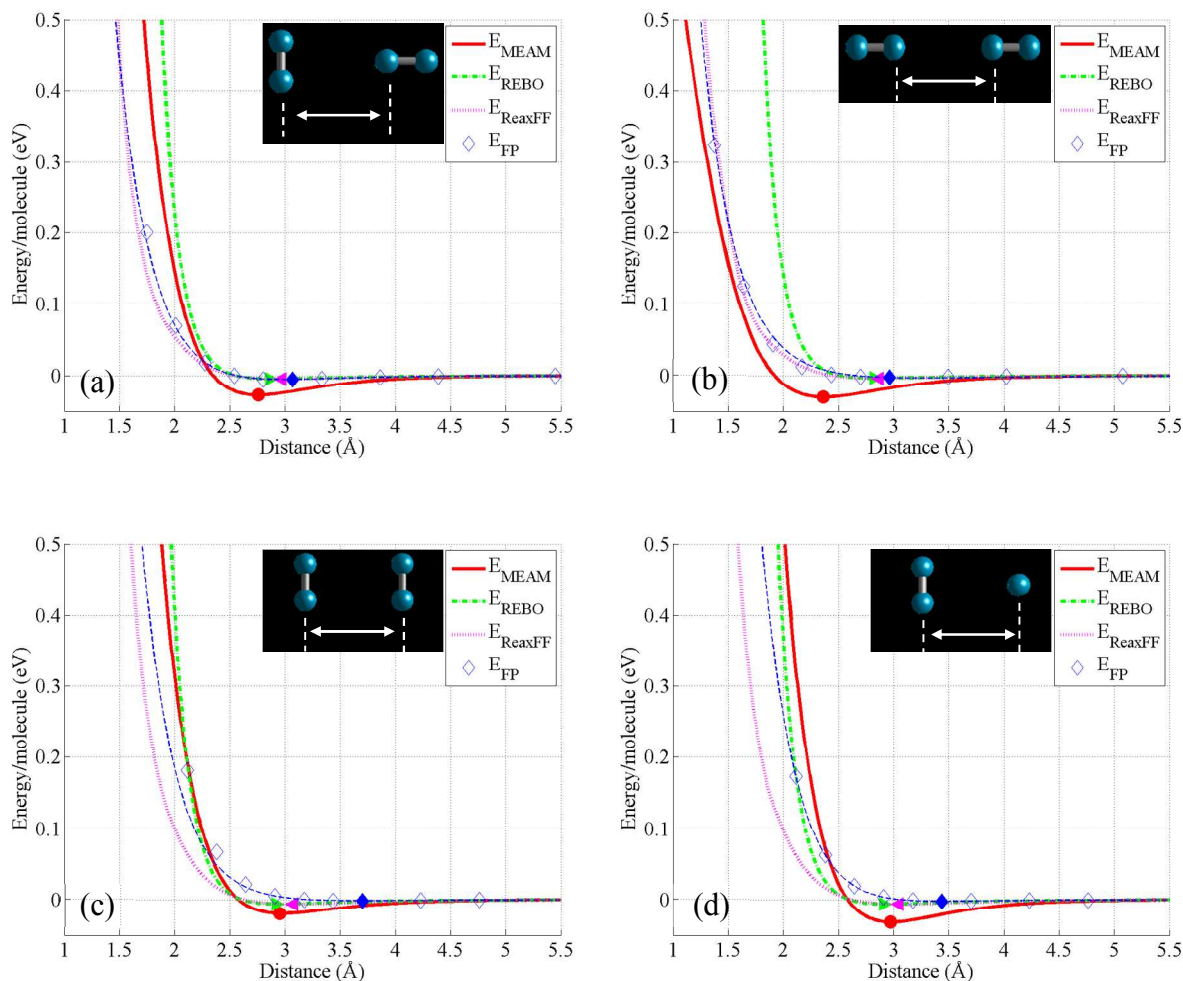


**Figure 6: Potential energy curves of a hydrogen dimer for MEAM, REBO, ReaxFF, and the FP data. The energy is relative to the energy at full dissociation. The molecular configurations are (a) collinear coplanar, (b) linear, (c) parallel, and (d) crossed as reported in the work of Burton and Senff.<sup>20</sup> The calculation method for FP is CEPA-PNO.<sup>26</sup> Filled markers indicate the minimum of each energy curve near the equilibrium intermolecular distance. The line that passes through the FP data serves as a guide. The atoms are constrained during the energy calculation at each distance increment. The white double arrows in the pictures of the molecules indicate the coordinate that is being varied, and the dashed lines represent the distance between the two molecules.**

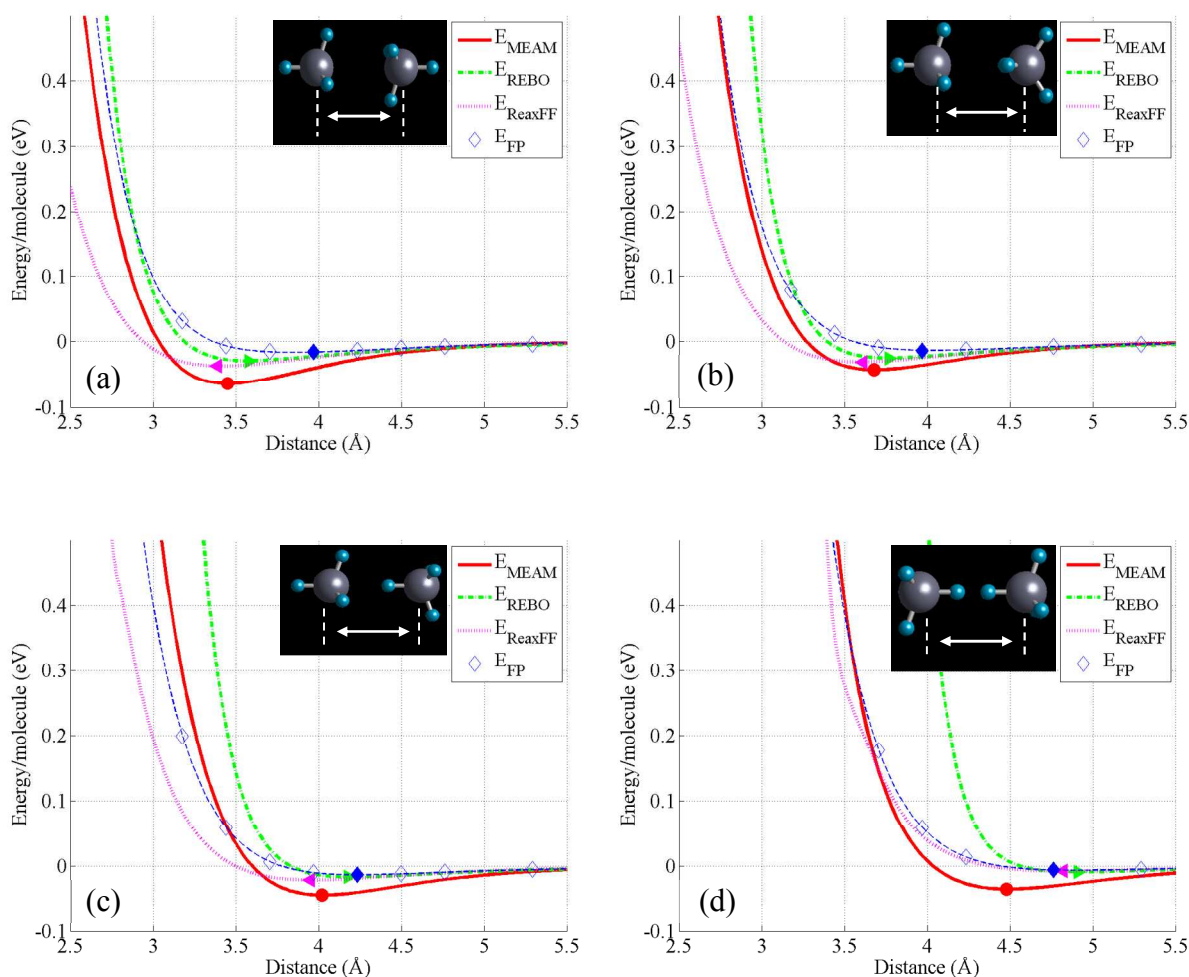


**Figure 7: Potential energy curves of a methane dimer for MEAM, REBO, ReaxFF, and the FP data. The energy is relative to the energy at full dissociation. The molecular configurations (a) A, (b) B, (c) D, and (d) F are reported in the work of Szczesniak *et al.*<sup>21</sup> The calculation method for FP is IMPPT/MPPT.<sup>27,28</sup> Filled markers indicate the minimum of each energy curve near the equilibrium inter molecular distance. The line that passes through the FP data serves as a guide. The atoms are constrained during the energy calculation at each distance increment. The white double arrows in the pictures of the molecules indicate the coordinate that is being varied, and the dashed lines represent the distance between the two molecules.**

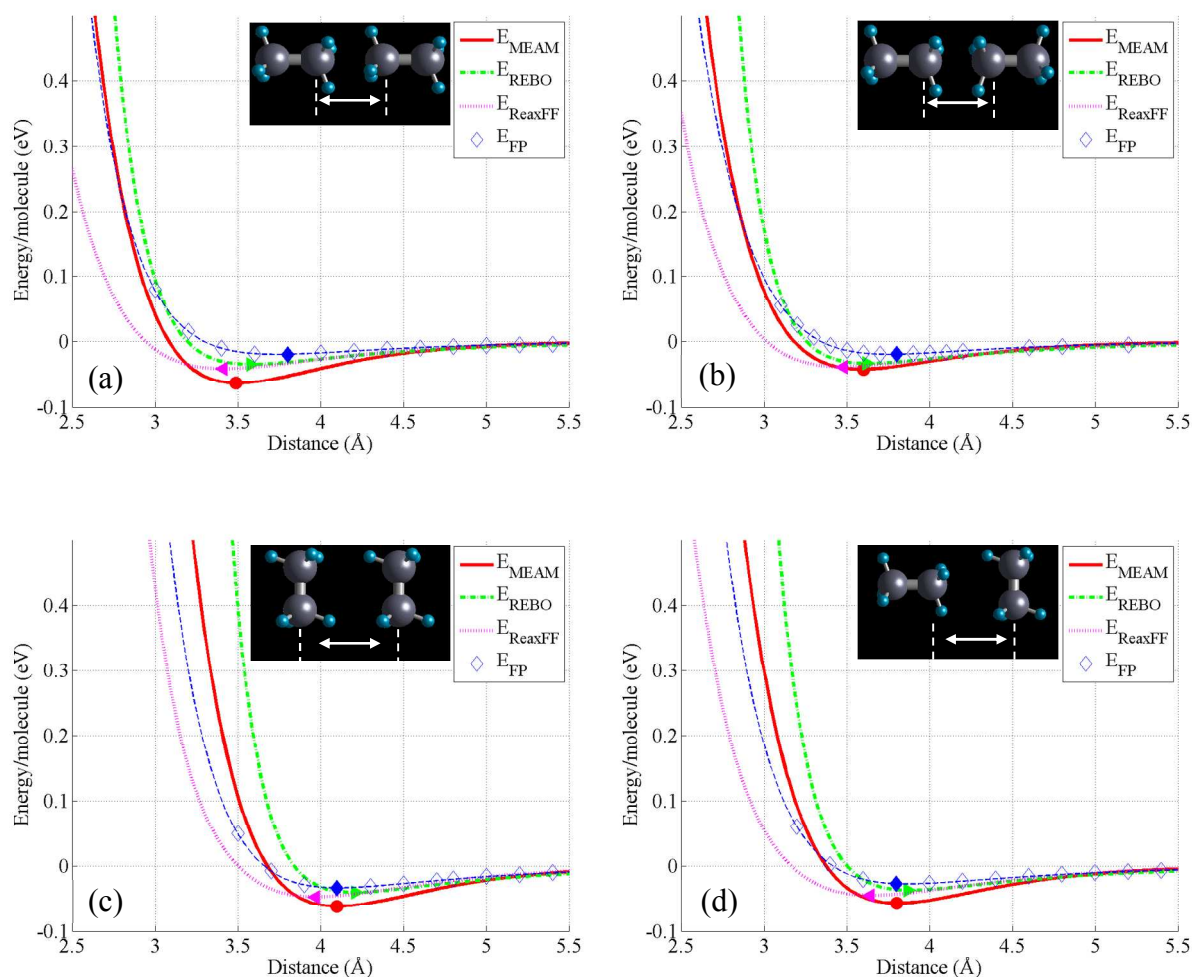


**Figure 8:** Potential energy curves of an ethane dimer for MEAM, REBO, ReaxFF, and the FP data. The energy is relative to the energy at full dissociation. The molecular configurations (a) Route 1, (b) Route 2, (c) Route 3, and (d) Route 4 are reported in the work of Rowley *et al.*<sup>22</sup> The calculation method for FP is MP2/6-311+G(2df,2pd).<sup>29,30</sup> Filled markers indicate the minimum of each energy curve near the equilibrium inter molecular distance. The line that passes through the FP data serves as a guide. The atoms are constrained during the energy calculation at each distance increment. The white double arrows in the pictures of the molecules indicate the coordinate that is being varied, and the dashed lines represent the distance between the two molecules.

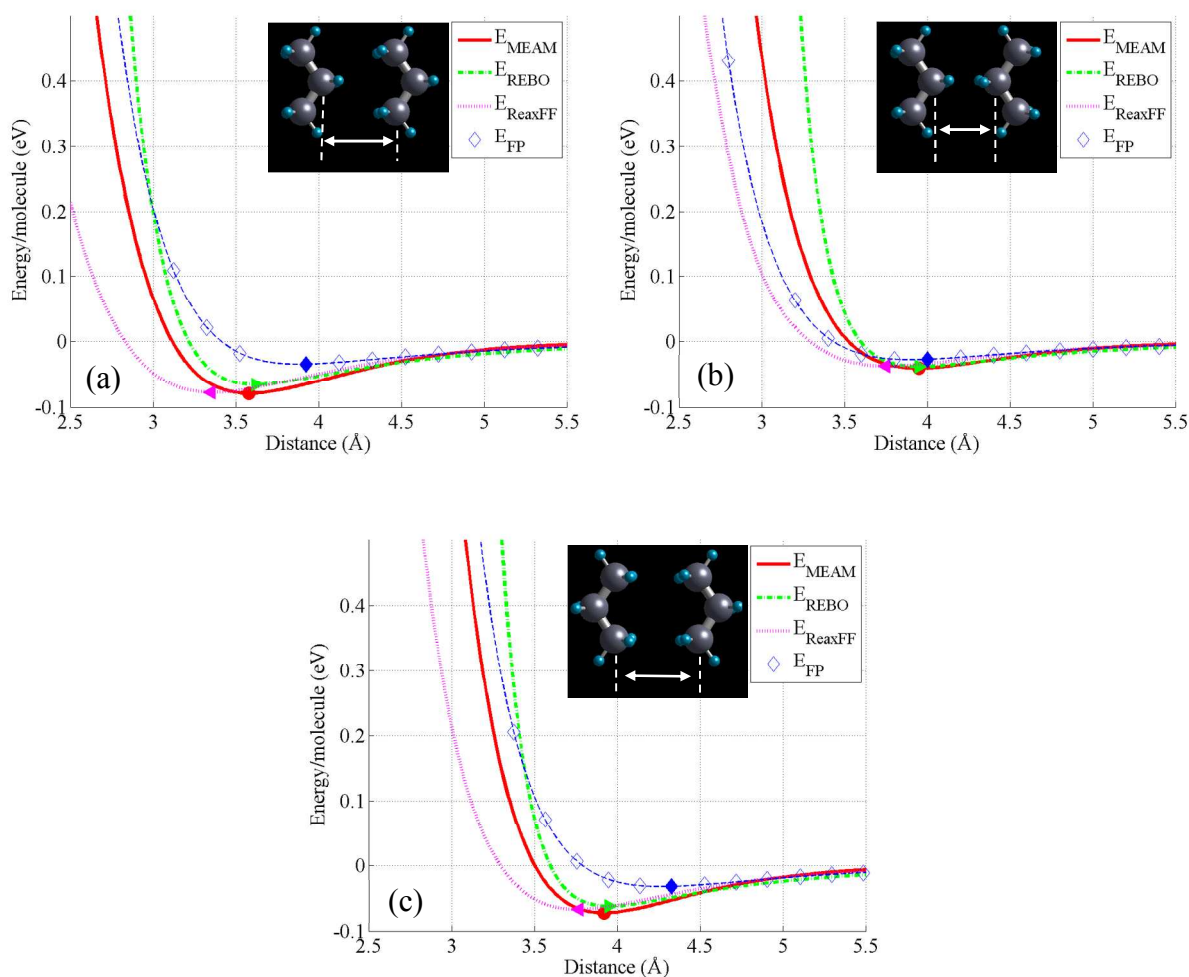


**Figure 9: Potential energy curves of a propane dimer for MEAM, REBO, ReaxFF, and the FP data. The energy is relative to the energy at full dissociation. The molecular configurations (a) bb-ccc 90, (b) bb-bb 90, and (c) ccs-ccs 90 are reported in the work of Jalkanen *et al.*<sup>23</sup> The calculation method for FP is MP2/6-311+G(2df,2pd).<sup>29,30</sup> Filled markers indicate the minimum of each energy curve near the equilibrium inter molecular distance. The line that passes through the FP data serves as a guide. The atoms are constrained during the energy calculation at each distance increment. The white double arrows in the pictures of the molecules indicate the coordinate that is being varied, and the dashed lines represent the distance between the two molecules.**

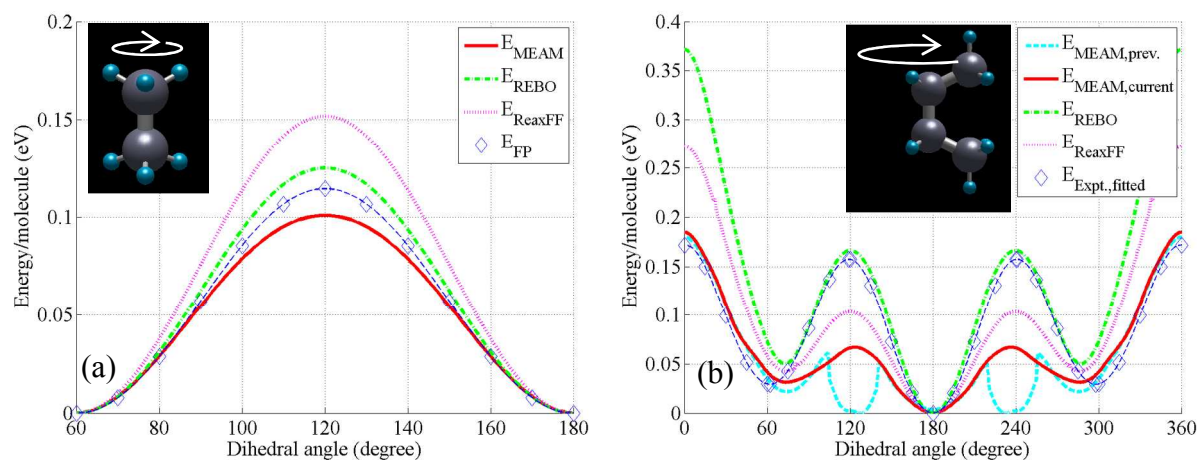
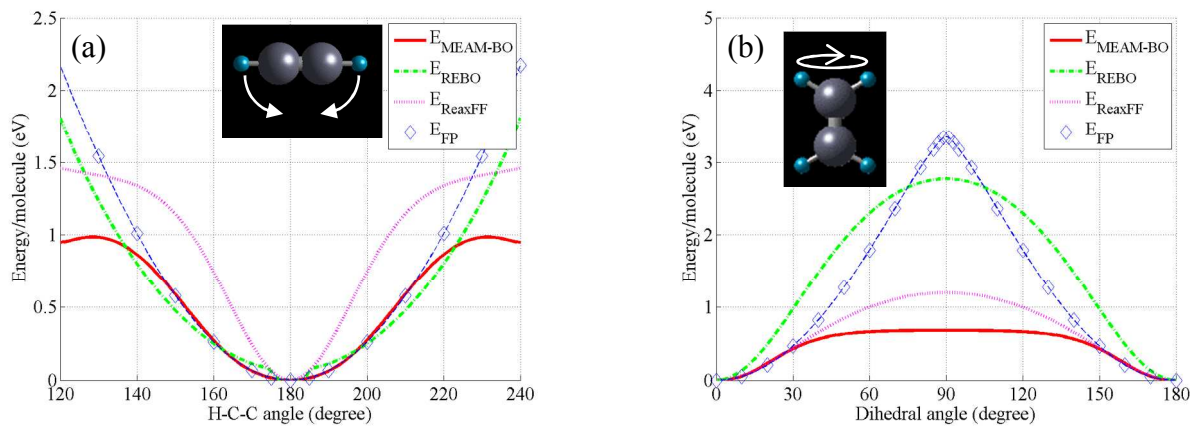


Figure 10: The rotational barrier for (a) ethane and (b) *n*-butane calculated by MEAM, REBO, ReaxFF, FP using (a)CCSD(2)/aug-cc-pVTZ<sup>24,25</sup> for (a) and the experimental data fit to a model for (b) from the work of Herrebout *et al.*<sup>32</sup> The white arrows in the pictures of the molecules indicate the coordinate that is being varied, and the line that passes through the FP or experimental data serves as a guide. The energy is relative to the minimum energy.



**Figure 11: (a) The bending barrier of acetylene and (b) the rotational barrier for ethylene calculated using MEAM-BO, REBO, ReaxFF, and FP using (a) CCSD(2)/aug-cc-pVTZ and (b) CCSD(T)/aug-cc-pVTZ.<sup>24,25</sup> The white arrows in the pictures of the molecules indicate the coordinate that is being varied, and the line that passes through the FP or experimental data serves as a guide. The energy is relative to the minimum energy.**

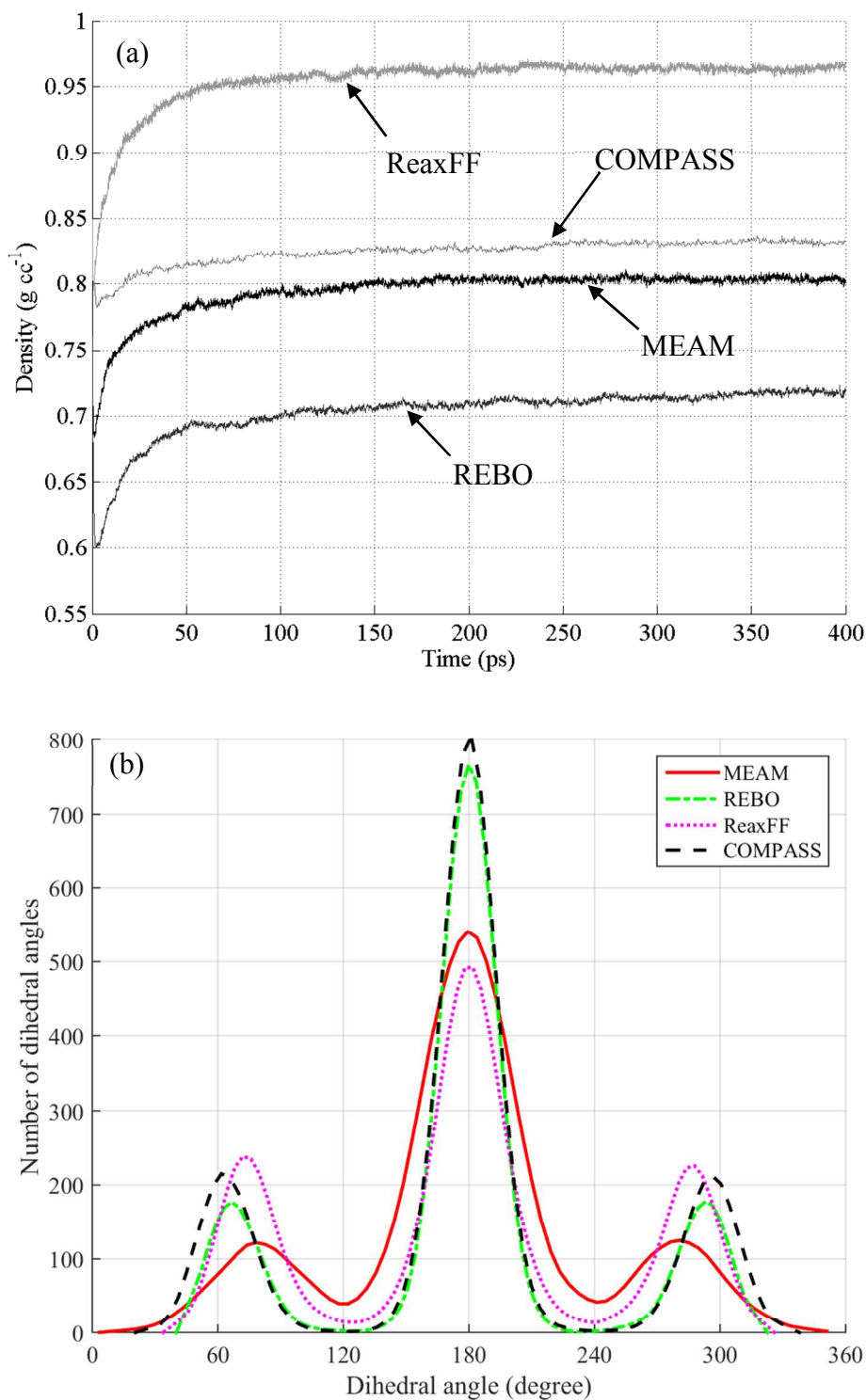


Figure 12: MD simulation using MEAM, REBO, ReaxFF, and COMPASS<sup>60</sup> potentials of (a) density versus time plot from an NPT simulation for amorphous polyethylene system with 20 chains of 250 monomers (30,040 atoms) with the initial density 0.85 g/cm<sup>3</sup> and (b) dihedral angle distribution of the system at 400 ps.

## TOC figure

